Next Materials 11 (2026) 101972

Contents lists available at ScienceDirect

Next Materials

journal homepage: www.sciencedirect.com/journal/next-materials

Research article

Wormwood-mediated green synthesis of iron oxide nanoparticles for antioxidant and antibacterial activities

Wanisa Abdussalam-Mohammed [a,*], Adel Younes [b], Mashael M. Alshaikh [c], Moussa Khlifa [b], Walaa Al-masri [d], Pawan Shah [e], Ajaya Bhattarai [f,*]

[a] Chemical Engineering Department, Faculty of Engineering, University of Tripoli, Tripoli, Libya
[b] Department of Chemistry, Faculty of Science, Sebha University, Sebha, Libya
[c] Department of Physics, University College in Al Jumum, Umm Al-Qura University, Saudi Arabia
[d] Department of Physics, Faculty of Science, University of Jeddah, Saudi Arabia
[e] Central Department of Chemistry, Tribhuvan University, Kirtipur, Nepal
[f] Department of Chemistry, Mahendra Morang Adarsh Multiple Campus, Tribhuvan University, Biratnagar, Nepal

ARTICLE INFO

Keywords:
Iron Oxide nanoparticles
2
2-diphenylpicrylhydrazyl
Acinetobacter *baumannii*
Staphylococcus aureus
Wormwood extract

ABSTRACT

For the first time, iron oxide nanoparticles (IONPs) with exceptional long-term stability at pH 7.6 were prepared using an aqueous *Wormwood* leaf extract. This unprecedented stability is of great importance in biomedical applications. The size and morphology of the iron oxide nanoparticles were studied using transmission electron microscopy (TEM), X-ray diffraction (XRD), zeta potential, and dynamic light scattering (DLS). Fourier transform infrared (FTIR) was used to identify the active functional groups in the extract that stabilized the iron oxide nanoparticles. Ultraviolet-visible (UV-Vis) spectroscopy showed a peak centered at 295 nm, confirming the successful preparation of iron oxide nanoparticles, which have stability of more than half a year. In this work, the stability of colloidal iron oxide nanoparticles was studied at different pH levels and temperatures, with a tendency to agglomerate at pH levels above 8.9 and below 6.5. The iron oxide nanoparticles had a size of 33 ± 2.5 nm, as determined by DLS analysis results. Furthermore, the zeta potential showed a positive charge of 44.32 mV, indicating excellent stability. Transmission electron microscopy (TEM) images revealed a spherical shape and a small size (17 ± 7.4 nm). The antioxidant activities were studied, and the results were 88.6% and 94.2% at the highest concentration (500 μg/mL) for both IONPs and aqueous artemisia extract, respectively. Furthermore, the IONPs exhibited good antibacterial properties against *Staphylococcus aureus* and *Acinetobacter baumannii* at concentrations (10, 30, and 60 μg/mL), better than the aqueous *Wormwood* extract at (0.0035 g/mL). The MIC was 30 μg/mL.

1. Introduction

Biomedical and environmental applications require highly stable nanoparticles, along with precise and controlled preparation conditions, using less expensive and hazardous materials and methods, to ensure biological efficacy and reliable therapeutic performance [1,2].

Recently, nanoscience has increasingly emphasized the development of environmentally friendly methods for synthesizing nanoparticles. Nanoparticle synthesis involves various techniques. Chemical and physical synthesis methods often involve high costs and significant energy consumption, generate hazardous byproducts, and use potentially flammable or toxic chemicals, raising environmental and biological safety concerns [3].

Hence, green nanotechnology is environmentally friendly, non-toxic, and safe for human health. Nanoparticles are synthesized using plant extracts rich in phytochemicals such as terpenoids, flavonoids, cinnamic acid, gallic acid, phenolic compounds, and so on [4]. The various compounds in the extract can perform various functions in the synthesis by acting as reducing, protecting, and stabilizing agents. Sustainable nanotechnology enables the synthesis of nanoparticles (NPs), such as iron oxide nanoparticles (IONPs), which have garnered significant interest due to their high surface area, magnetic properties, cost-effectiveness, and broad applications, such as wastewater treatment [5], antimicrobial, antioxidant, anticancer, and drug delivery

* Corresponding authors.
E-mail addresses: w.ahweelat@uot.edu.ly (W. Abdussalam-Mohammed), ajaya.bhattarai@mmamc.tu.edu.np (A. Bhattarai).

https://doi.org/10.1016/j.nxmate.2026.101972
Received 3 December 2025; Received in revised form 17 March 2026; Accepted 23 March 2026

capabilities. This makes them useful in diverse fields such as electronics and agriculture [6]. Many plant extracts have been used in the preparation of IONPs, including Melaleuca sophila [7], eucalyptus leaf [8], Tridax procumbens [9], Callistemon viminalis, Sida cordifolia, and rosemary officinalis, etc. [10].

Therefore, the main concern lies in the lack of innovation and manufacturing highly stable, over a significant span of time, iron oxide nanoparticles to prevent the development of microbial resistance to antibiotics and ensure their safe use in biomedical, clinical, and agricultural applications.

Among the plant extracts is *Wormwood*, also known as Artemisia absinthium L, which is an aromatic herb found throughout the temperate zone. Recent research has shown that it eliminates malaria parasites; it is extensively used in medicine to treat many diseases, due to its antifungal, neuroprotective, insecticidal, and antimicrobial properties. It is also an anthelmintic, antidepressant, hepato-protective, and treats stomach problems [11,12]. The reason to choose this plant in this study because containes important biocompounds, including flavonoids (myricetin, rutin, quercetin, hesperidin), hydroxycinnamic acids (caffeic acids, ferulic acid, coumaric acids), and hydroxybenzoic acids (gallic acid, salicylic acid), as illustrated in the literature [13].

Furthermore, *Wormwood* contains numerous bioactive compounds, such as santonin, which has anti-inflammatory, antidiabetic, antitumor, antioxidant, and antiparasitic properties. In addition, it has garnered significant attention due to its anti-inflammatory effects. For example, clinical studies have indicated positive effects in the treatment of Crohn's disease. Patients receiving an herbal mixture containing *Wormwood*, in addition to standard steroids, can reduce their steroid dosage; disease remission has been observed in 65% of patients after eight weeks of treatment [13]. Artemisinin is the main component of most *Wormwood* species, and the phytochemicals present in *Wormwood* can act as natural reducing and stabilizing agents for the synthesis of IONPs [14]. Where a previous study confirmed the presence of six methoxylated flavones in the *Wormwood* extract, including jaceosidin, eupatilin, hispidulin, acacetin, eupatorin, and casticin by using the LC-MS technique [15].

According to the recent study [13], HPLC-DAD analysis of *Wormwood* was performed to identify polyphenols the polyphenols, and the results showed the presence the following polyphenols: protocatechuic acid (0.10 ± 0.01 mg/g), chlorogenic acid (5.72 ± 0.11 mg/g), caffeic acid (2.07 ± 0.01 mg/g), ferulic acid (19.57 ± 0.44 mg/g), rosmarinic acid (7.82 ± 0.01 mg/g) [13].

IONPs have been prepared with *Wormwood* extract before, but, to our knowledge, based on previous studies, no study has addressed the stability time of IONPs prepared with *Wormwood* extract. None of the previous reports on IONPs prepared from aqueous *Wormwood* extract has provided a clear and comprehensive methodology that highlights the role of both temperature and pH during the preparation process and their impact on the structural and morphological properties of IONPs. Only, most studies focused mainly on basic synthesis and characterization. For example, IONPs prepared with African *Wormwood* (Artemisia afra) leaf extract are stable within a size range of 15–20 nm [16].

Moacă et al. [10]. prepared aqueous extracts of *Wormwood* (Artemisia absinthium L.) leaves to produce highly stable spherical monolayers with a size range of 1–10 nm [10]. Similarly, small-sized monolayers (2.15 nm) were prepared by El Ghanjaoui et al. [17]. using *Wormwood* leaf extract as a stabilizer and bio-reducing agent, and applied to the degradation of tartrazine and Nile Blue A (NBA) dyes, demonstrating high efficiency in the degradation of tartrazine and Nile Blue dyes [17]. Similarly, single ions smaller than 30 nm, stabilized with Artemisia vulgaris leaf extract, were used as catalysts for the degradation of methyl orange (MO) dye in water, and the results significantly reduced the total organic molecules [18].

In addition, Artemisia afra catalyzed ion particles with sizes of 31 and 24 nm, which showed significant antibacterial activity against Escherichia coli, Chromobacterium violaceum, *Pseudomonas aeruginosa*, and *Staphylococcus aureus* [19].

There are different methods of synthesis of IONPs mentioned in the above literature. However, there is always a demand for green synthesis of NPs that should be eco-friendly, sustainable, cost-effective, and simple. Along with that, the prepared NPs should be stable at low and high temperatures, low and high pH values, and for a long period of time. In this study, IONPs are synthesized with *Wormwood* extract in simple and cost-effective ways, and their stability has been maintained for more than 6 months, which brings their huge applications in the biomedical, catalysis, and metal separation techniques.

Our study aims to prepare highly stable, biocompatible IONPs by a safe, green method to enhance their biomedical applications, especially their antibacterial and antioxidant activities, providing new insights for improvement.

2. Experimental

2.1. Materials and methods

Pure and analytical chemicals in this work were used directly without any additional purification. Ascorbic acid ($C_6H_8O_6$) and ferric chloride hexahydrate ($FeCl_3$. 6 H_2O) were obtained from Carlo Erba, France. NaOH, HCl, ethanol, and acetone were purchased from Sigma-Aldrich (USA). High-purity DPPH was purchased from MACKLIN, China.

All glassware (conical flasks, measuring cylinders, beakers, petri plates, and testers (Pipes, etc.) was purchased from Fisher Scientific, UK.

2.1.1. Preparation methods

In this work, the synthesis of biocompatible Iron Oxide nanoparticles (IONPs) was carried out using the aqueous extract of medicinal plant leaves (*Wormwood*).

2.1.2. Preparation of plant extract

The *Wormwood* plant extract was prepared using the heated maceration (assisted maceration) method, with a few minor modifications [10]. The *Wormwood* leaves plant was purchased from the commercial markets in Sebha city, southern Libya. The plant materials used in this study were collected and documented by a taxonomist in the Department of Botany, Faculty of Science, University of Sebha, Libya. A voucher sample was deposited in the department's herbarium for reference. The leaves were collected and cleaned multiple times. To get rid of any dirt accumulation, they were first rinsed with tap water and then repeatedly rinsed with distilled water. The leaves were dried in the shade for a week, then ground using an electric grinder to obtain fine

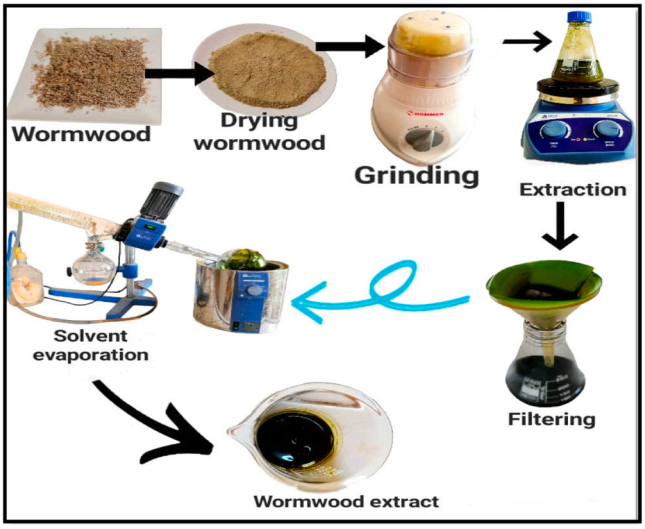

Fig. 1. A step-by-step guide for preparing *Wormwood* leaf extract.

powder as illustrated in Fig. 1. A (200 mL) mixture of (10 mL) ethanol and (190 mL) deionized distilled water was added to the soft powdered leaves of *Wormwood* (75 g) in a 1-liter beaker. After that, the mixture was magnetically agitated and heated for four hours at 40 °C. This moderate temperature was intentionally chosen to enhance solvent penetration, diffusion, and extraction efficiency of biologically active compounds, while keeping it sufficiently low to avoid thermal degradation of heat-sensitive plant chemicals.

The extract solution turned dark green instead of bright green. After filtering the extract using Whatman filter paper, it was centrifuged for an hour at 1250 rpm. A rotary evaporator was used to concentrate the *Wormwood* extract at 40°C to remove any residual solvents, water, and ethanol (EtOH) that might remain in the precipitate. The prepared extract was then dried and stored in the dark until use.

2.1.3. Synthesis of IONPs using the extraction of Wormwood

Iron oxide nanoparticles (IONPs) were synthesized via a green reduction method using *Wormwood* (*Artemisia absinthium L.*) leaf extract as reducing and capping agent, following previously reported approaches with minor modifications [10,20]. Briefly, 0.009 g of ferric chloride ($FeCl_3$. 6 H_2O) was dissolved in 20 mL of deionized water to prepare the iron precursor solution (0.0333 mmol). Separately, an aqueous plant extract solution (3.47 mg/mL) was prepared by dissolving 0.052 g of the dried *Wormwood* extract in 15 mL of deionized water.

For nanoparticle synthesis, 15 mL of the $FeCl_3$. 6 H_2O solution was mixed with 5 mL of the *Wormwood* extract solution, corresponding to an extract-to-precursor volume ratio of 1:3. The mixture was stirred continuously at room temperature for approximately 2 h. Subsequently, the pH of the reaction mixture was adjusted from 6.0 to 7.6 by the dropwise addition of 0.1 M NaOH under constant stirring.

A visible colour change from brown to blackish-brown was observed, indicating the reduction of Fe^{3+} to Fe^{2+} ions and the formation of iron oxide nanoparticles [20]. The blackish-brown colour remained stable after 4 h of reaction, confirming nanoparticle formation and stability (Fig. 2). Similar colour changes during the biosynthesis of iron oxide nanoparticles using *Artemisia* species have been reported in the literature, supporting the successful formation of IONPs [15, [21].

2.1.4. Stability study

The stability of the produced IONPs was monitored in acidic and basic environments. The impacts of different pH levels and temperatures on the stability of the produced colloidal IONPs were investigated in this study; stability is determined by careful monitoring of any change in spectral absorption (UV-Vis) as well as the change in SPR peak intensity. Different colors of synthesized IONPs were noticed at different pH values.

2.1.4.1. Effect of pH Values. The extent of the effect of adding HCl (0.1 M) or NaOH (0.1 M) (5–25 µL) on the spontaneity of the prepared IONPs was carried out in this study. As is known, nanoparticles have a specific pH at which they are formed that demonstrates their stability [22,23]. For instance, increasing or decreasing the pH values leads to a loss of dispersion of nanoparticles. The amounts of HCl or NaOH were added (5–25 µL) to IONP solutions to raise their pH values. The solutions were stirred for about 5 min after each addition, and the SPR was measured by UV-Vis spectrophotometer.

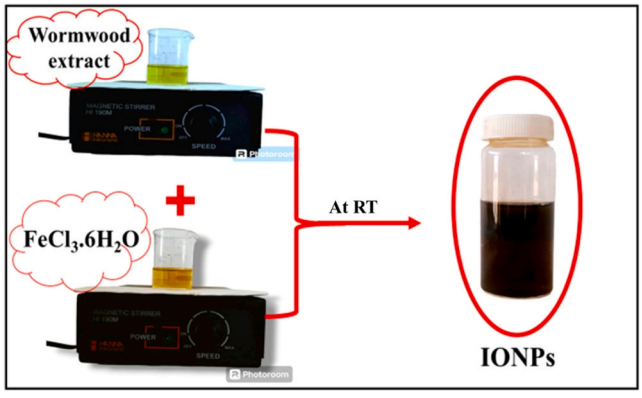

Fig. 2. Process of IONPs prepared by *Wormwood* leaf extract at room temperature.

2.1.4.2. Effect of temperature values on the stability of IONPs. The synthesis of IONPs can be affected by temperature, as demonstrated in different research [24,25]. Consequently, the stability of IONPs was examined at room temperature and at different temperatures, including 40 °C, 60 °C, and 90 °C.

2.2. Characterization of iron oxide nanoparticles

2.2.1. X-ray diffraction (XRD) analysis

Herein, the X-ray diffractometer (made in Germany) is employed to study crystalline metallic IONPs. The XRD analysis was performed using Rigaku DMAX 2100 diffractometer at 40 mA and 40 kV, utilizing Cu-Kα1 radiation with a monochromatic filter at a wavelength range of 1.54 A°. The biosynthesized IONPs were completely dried in powder form before being placed in the XRD apparatus cube.

2.2.2. Ultraviolet visible spectroscopy (UV-Vis)

The surface plasmon resonance (SPR) of IONPs was achieved in the range between 200 nm and 800 nm. The UV-Vis (Model: Evolution 300, Thermo Fisher Scientific, UK) was used for this purpose at R.T. The quartz cuvette cell (Fisher Science, USA) with a length of 1.0 cm was used, and samples were diluted with distilled H_2O at a ratio of 1:3. UV-Vis spectra were collected by loading 3.5 mL of the IONPs sample into a quartz cuvette cell. The spectrophotometer spectrum was corrected using a blank sample (distilled water).

2.2.3. Fourier transform infrared spectroscopy (FT-IR) analysis

Fourier transform infrared spectroscopy (FTIR) is an effective technique applied to measure and identify the important functional groups of the extract that is used to functionalize the nanoparticles. The solid sample was mixed and hard-pressed with 150 mg of KBr. The scan was recorded at wavenumber from 4000 cm^{-1} to 400 cm^{-1}using a Bruker Vertex 70.

2.2.4. Dynamic light scattering (DLS) and zeta potential analysis

The colloidal IONPs were examined by a DLS device (NICOMP 380 ZLS, USA) at the National Security Center Laboratory, Cairo, Egypt, where the 632 nm of a helium-neon (HeNe) laser line was used as the incident light at an angle of 90 °, while the zeta potential was measured at an external angle of 18.9 °. The dispersed IONP was analyzed after dilution (1:1) in distilled H_2O. The measurements were carried out three times for better accuracy. All measurements were performed in automatic mode at 25 °C.

2.2.5. Transmission electron microscope (TEM)

The size of IONPs was examined by the National Security Center Laboratory, Cairo, Egypt, where TEM micrographs of IONPs were prepared by dropping dispersed IONPs on a carbon-coated copper grid (S160–3 Plano GmbH), and it was observed by using a JEOL 120/JEOL 200 TEM (Carl Zeiss NTS) set at 120 kV/200 kV. For the preparation of transmission electron microscopy (TEM) samples, IONPs were deposited by dripping a dilute solution onto a carbon-coated copper grid, followed by evaporation of the solvent under ambient conditions [26]. This drying process may contribute to partial particle shrinkage, flattening, or removal of the solute/coating layer, resulting in smaller apparent particle sizes compared to those measured in the aqueous state using

dynamic light scattering (DLS). Furthermore, TEM provides a two-dimensional projection of three-dimensional particles, which may also contribute to size variations [27].

2.3. Antioxidant activity using 2, 2-Diphenylpicrylhydrazyl (DPPH) radical-scavenging assay

Metal oxides are gaining momentum in inorganic catalysis and photocatalysis, driving the development of environmentally friendly methods [28]. The antioxidant activity of biocompatible IONPs was measured in this study, following the same approach as in previous studies, with some modifications. DPPH is widely used as a free radical in model systems to study the detoxification activity of metal /metal oxide nanoparticles [29].

The ability of IONPs and *Wormwood* leaf extract to detoxify metals using DPPH was evaluated. Briefly, 0.0010 g of DPPH was dissolved in ethanol (25 mL) and stored in the dark. Study samples (*Wormwood* extract and IONPs) were then prepared at different concentrations (200, 300, 400, and 500 μg/mL) to which 200 μL of DPPH solution was added. Additionally, 200 μL of a solution containing only DPPH in 200 μL of ethanol was used as a standard (control), and ascorbic acid was used as a reference at concentrations similar to the study samples. The tubes were then left in complete darkness for 30 min. DPPH removal activity was measured using a UV-Vis spectrometer (Model: GENESYS 10 UV, Thermo Scientific Scanning, USA), where the absorbance was determined at a wavelength of 517 nm. Free radical scavenging was measured using the following formula:

antioxidant activity (%) = (Control - Sample / Control) × 100 [21].

2.4. Time-kill curves of anti-bacterial activity of dispersed IONPs

The time–kill assay in this work was carried out following the process described in the literature [30]. The super sensitivity of the produced IONPs is defined by optical density measurements (OD). The samples were incubated for 6 h at 37°C, and the OD of examined samples at 600 nm (OD600) was analyzed at a variety of incubation times of 0, 1, 2, 3, 4, 5, and 6 h using a Jenway 6305 UV/Vis spectrophotometer (UK). The antibiotic (Daptomycin and meropenem 10 μg) was used as a control with the IONP samples against bacterial strains of Gram-negative (*A. baumannii*) and Gram-positive (*S. aureus*) bacteria. Iron oxide nanoparticles (IONPs) were prepared to test their antibacterial activity as follows: First, a concentrated suspension of IONPs was prepared at a high concentration of 60 μg/mL. The suspension was then subjected to ultrasound for 15 min using a sonicator equipped with a probe to ensure homogeneous dispersion and prevent the nanoparticles from aggregating. Subsequently, different dilute solutions were prepared at concentrations of 30 and 10 μg/mL of IONPs. After six hours of incubation, OD600 was used to evaluate bacterial growth inhibition. The resulting data were drawn using GRAPHPAD PRISM V5.00 software (ANOVA test) ($p < 0.05$).

2.5. Determination of MIC by broth microdilution method

The Minimum Inhibitory Concentration (MIC) was defined as the lowest concentration of a compound that prevents visible bacterial growth. MICs of IONPs *against Staphylococcus aureus* (Gram-positive) and *Acinetobacter baumannii* (Gram-negative) were determined using a broth microdilution assay in 96-well plates (Greiner-Dio-One). Absorbance was measured at 600 nm using a BioTek Synergy H1 multi-mode spectrophotometer.

Nutrient Broth (NB) was prepared from dehydrated powder and sterilized by autoclaving at 121 °C for 15 min. Bacterial cultures were adjusted to ~ 1.5×10^8 CFU/mL (0.5 McFarland standard). IONPs solutions were filtered through 30 μm syringe filters and tested at three concentrations: 10, 30, and 60 μg/mL. Each concentration was mixed with bacterial inoculum in NB medium and incubated at 37 °C for 24 h. The positive control indicated the NB medium with IONPs but without inoculum, while the negative control refers to NB medium with inoculum but without IONPs

Optical density (OD) readings of samples were corrected by subtracting the corresponding positive control values. Each experiment was performed in three replicates, and the mean ± standard deviation of OD was calculated to assess bacterial growth inhibition [31].

The inhibition percentage was calculated by the equation below:

$$\text{Inhibition } (\%) = \frac{OD_{control} - OD_{sample}}{OD_{control}} \times 100$$

3. Results and discussion

3.1. Characterization of iron oxide nanoparticles

3.1.1. X-ray diffraction analysis of green-synthesized IONPs

XRD measurements were used to confirm the crystallinity of nanoparticles by analyzing their diffraction patterns. Herein, the biocompatible IONPs exhibited a crystalline structure. The complete XRD spectrum of 2θ readings ranged from 20 to 80°, where the XRD spectra confirmed the formation of IONPs by detecting four distinct peaks that matched the standard card (JCPDS card No. 00–005–0628). The X-ray displays well-defined Bragg reflection characteristics of Fe_3O_4, and diffraction angles of IONPs obtained at 2θ were ~ 31.4°, 45.4°, 56.7°, and 75°, corresponding to the (222), (400), (511), and (553) planes, respectively, as shown in Fig. 3.

These reflection peaks have been attributed to the magnetite structure of iron oxide nanoparticles in previous studies [21,32–36]. The high intensity and sharpness of these peaks also indicate the crystalline nature of the green synthesized IONPs. Additionally, the XRD pattern displays sharp and distinct patterns, which are also in agreement with previous observations [37]. In contrast to our study, a previous investigation reported that IONPs prepared using Urtica dioica leaf extract showed no noticeable diffraction peak throughout the pattern, indicating that the green synthesis approach using plant extract led to the generation of amorphous IONPs [38]. Another study confirmed the

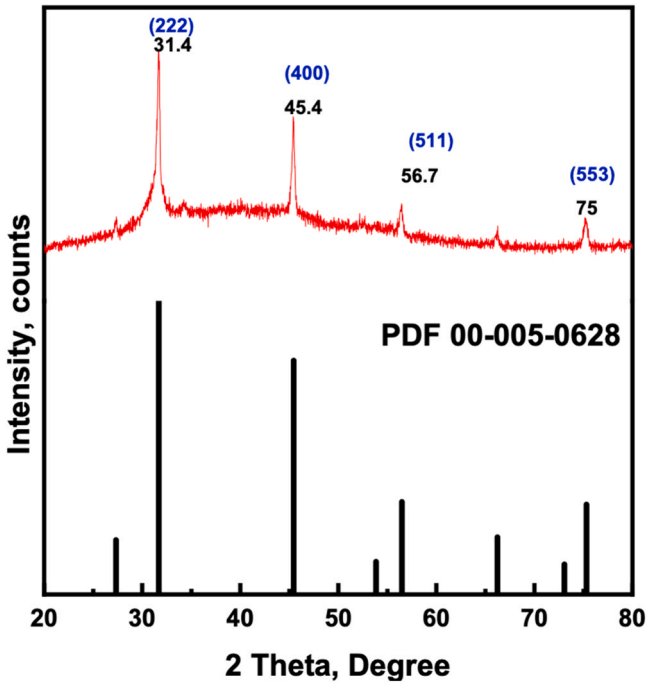

Fig. 3. X-Ray diffraction pattern of IONPs functionalized by *Wormwood* extract. The crystal size of IONPs obtained from XRD measurements after storage, approximately two months after synthesis.

absence of distinctive diffraction peaks, indicating that the IONPs are amorphous [39].

In our study, a single phase of iron oxide was obtained, which is magnetite, considered one of the best families of iron oxides according to the description of the previous study [8]. In addition, the purity of the present IONPs sample was demonstrated by the absence of additional peaks, indicating high purity, meaning only the desired phase is present. It has been mentioned in the previous literature [39] that the appearance of additional peaks that do not match the reference card may be due to other forms of iron oxides or magnetite in the samples, or because of the presence of organic functional groups from the leaf extract that are responsible for covering and controlling the nanoparticles' properties [39]. The average crystal size was evaluated and quantified using the Debye-Scherrer equation, with its average crystal size found to be ~ 50.4 nm, as shown in Table 1. The large size of the crystal may indicate a crystallite cluster; its value is larger than the particle size observed by TEM (~17 nm), which can be attributed to the difference between the individual particle size and the size of coherently diffracting crystalline domains.

The crystallite size (D) is calculated from the well-known Debye-Scherrer's formula [40],

Where the Debye-Scherrer Eq. (1) is used to calculate the average crystalline size of the produced IONPs after two months from preparation.

$$D = \frac{K\lambda}{\beta hkI \cos\theta hkI} \quad (1)$$

where:

K= 0.95–098 (shape factor)

λ= 0.145 nm (X-ray wavelength)

β_{hkI} = is the line broadening at half the maximum intensity (FWHM) (radians)

θ_{hkI} = Bragg- diffraction angle (peak position in radians)

TEM analysis was performed immediately after synthesis and reflects the size of well-dispersed individual NPs, whereas XRD measurements were conducted after approximately two months of storage. During this storage period, IONPs, due to their high surface energy and strong magnetic dipole–dipole interactions, are prone to agglomeration and partial crystallite coalescence [41]. Such aggregation can lead to the formation of larger crystallite clusters or oriented attachment of primary nanoparticles, resulting in an increased apparent crystallite size as determined by XRD.

According to Shaik et al. [40]. the crystallite size of the particles differs slightly from the size of the particle as results to the formation of poly-crystalline aggregates [40].

Consequently, the larger crystallite size obtained from XRD does not contradict the TEM results but rather reflects post-synthesis aggregation and crystallite growth during storage.

3.1.2. Ultraviolet-visible (UV-Vis) spectroscopy investigation

The produced colloidal iron oxide nanoparticles were easily confirmed by UV-Vis spectroscopy. As is known, UV-Vis spectroscopy offers information about the size, aggregation, and surface chemistry of the NPs [27]. This technique also validates the synthesis of IONPs as well as the stability of nanoparticles. The wavelength of the spectrometer was tuned between 200 and 800 nm. Nanoparticles have remarkable optical properties, and these capabilities are sensitive to size, shape, agglomeration state, concentration, and surface, making spectroscopy a valuable tool for identifying and characterizing nanoparticles. IONPs interact strongly with specific wavelengths of light due to their optical properties. Herein, UV-Vis spectra were collected by loading 3.5 mL of the IONPs sample into a quartz cuvette cell (Fisher Science, USA). The spectrophotometer spectrum was corrected using a blank sample (distilled water). In this study, a strong, narrow peak was observed in the UV-Vis spectrum at 295 nm of IONPs, indicating the successful production of dispersed IONPs due to the complete reduction of Fe^{3+} to Fe^{2+}. The narrow peak in the spectrum indicates the formation of monodispersed IONPs. Iron oxide nanoparticles synthesized by plant extract are known to exhibit a maximum UV-Vis absorption in the range of 240–360 nm due to surface plasmon resonance (SPR) [42]. SPR is highly dependent on particle properties. In general, the particle sizes and shapes of IONPs are impacted by several factors, including pH variation, stirring rate, and temperature during the synthesis process [13,43].

Iron oxide nanoparticles exhibit strong plasmonic properties. The interaction of light photons with their metallic surfaces excites free electrons into a state of oscillation. When exposed to certain wavelengths of light, the motion of these free electrons synchronizes with the light wave, resulting in a transition to an absorption band known as surface plasmon resonance (SPR). This phenomenon happened as a result of the combined vibration of the electrons in the nanoparticles' ionic bands, which resonates with the light wave [43]. In this way, the concentration of the reducing agents, in addition to the concentrations of the metal itself, plays a crucial role in the production and improvement of IONPs, and such results have also been reported for iron oxide nanoparticles from *Wormwood* [32].

3.1.3. Fourier transform infrared spectroscopy (FT-IR) results

The aim of using the FT-IR spectroscopy is to investigate the positions of the active functional groups that functionalized IONPs and should be present on their surface, and to identify the important functional groups that participated in the processes of reduction, coating, and stabilization of IONPs. It also aims to compare all the changes that have occurred.

3.1.4. Infrared spectra results of wormwood leaf extract

Each spectrum was recorded with 32 scans at a resolution, and the spectral range covered was 4000–400 cm^{-1} . The findings of this work exhibited the active role of the active groups present in the *Wormwood* leaf extract. For example, the broadband at about 3254 cm^{-1} in the extract is related to the OH hydroxyl group (phenols or alcohols), or amines (N-H stretching), similar to other studies [44]. The peak bands at positions 1637 cm^{-1} and 1467 cm^{-1} belong to the aromatic alkene (-C═C stretching) and carbonyl group (-C═O stretching), respectively. The C═O was shifted to a low peak as a result of its conjugation with the double bond of the aromatic bond in the flavonoid [45], as illustrated in Fig. 4.

In addition, Fig. 5A shows the FT-IR spectra of *Wormwood* leaf extract, where the peak at 1177 cm^{-1} refers to the presence of ether or

Table 1
Average crystallite size of IONPs from Debye-Scherrer's ($D = K\lambda/\beta hkI \cos\theta hkI$).

Peak Position(2θ)	FWHM (β)	Size (nm)
66.053	0.307	30.85223248
75.170	0.276	36.30824574
27.212	0.100	81.70488599
56.339	0.100	90.08168679
45.416	0.270	31.88329248
31.660	0.260	31.74705553

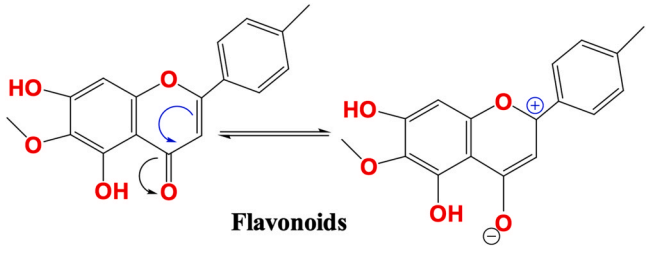

Fig. 4. Prediction resonance of flavonoids.

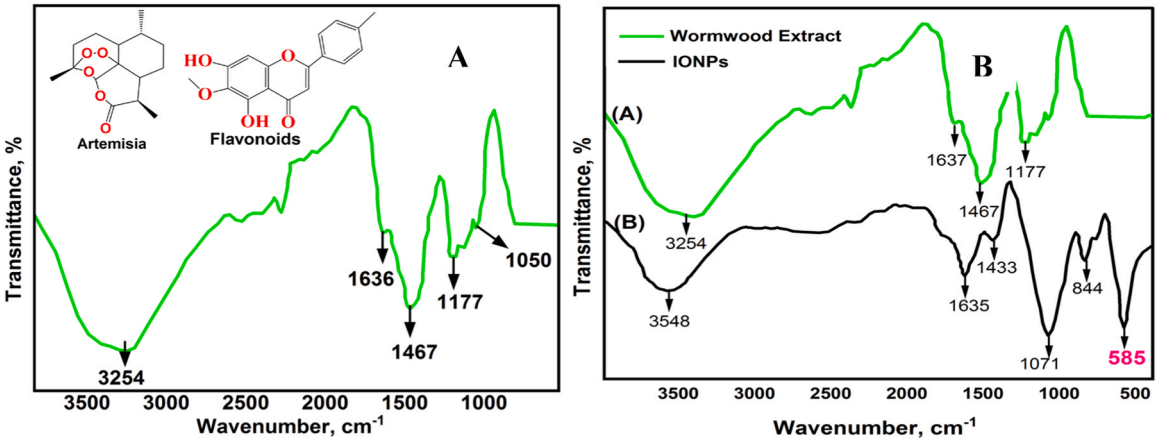

Fig. 5. (A) FT-IR spectrum result of *Wormwood* extract, (B) FTIR spectra comparing *Wormwood* leaf extract (green curve, A) and IONPs functionalized by the mentioned extract (black curve, B).

glycoside groups (-R-O-R) in the extract, while the weak peak at 1050 cm^{-1} corresponds to the alcohol group (C-O stretching), similar to those reported [45].

According to Mamatova et al. [46]. the ESI-TOF-MS/MS spectrum of *Wormwood* extract exhibited about 13 compounds, with molecular ion peaks are shown at m/z = 161.0229, 353.0889, 609.1494, 515.1207, 515.1209, 377.0817, 193.0491, 161.0241, 285.0406, 315.0513, 269.0450, 329.0679 identified as umbelliferon, chlorogenic acid or its isomer, rutin, dicaffeoylquinic acid isomer, scopolin, 4-hydroxycoumarin, 3-hydroxycoumarin, luteolin, isorhamnetin, apigenin, rhamnazin, respectively [46].

3.1.5. Infrared spectra results of IONPs functionalized by wormwood leaf extract

Fig. 5B depicts the spectra of IONPs functionalized by *Wormwood* leaf 4 extract. After preparing IONPs using *Wormwood* leaf extract, very slight changes and displacements occurred in the positions of the functional groups. This indicates the presence of these groups on the nanoparticle surface; a shift occurred in the peak at 3548 cm^{-1} in IONPs, which was at 3254 cm^{-1} in the case of the extract sample. This peak is due to the OH^- group that contributed to the reduction process and stabilized IONPs. The absorption band at 1635 cm^{-1} in IONPs is attributed to the carbonyl group (C═O stretching); this peak had a slight shift in the extract and was at 1637 cm^{-1} . Additionally, the absorption band at 1467 cm^{-1} in *Wormwood* extract was shifted to 1433 cm^{-1} in IONPs is attributed to aromatic alkene (C═C stretching). Meanwhile, the absorption band at 1177 cm^{-1} in the extract corresponds to the ether group (C-O-C), where a clear change and shift occurred, as this peak was present in the IONPs at the vibrational range of 1071 cm^{-1} , which confirms that it participated in the reduction process and capping of IONPs.

The most important peak that confirms the successful preparation of IONPs was at 585 cm^{-1} , and this range is specific to Fe-O. This result is consistent with the previous literature [47] mentioned the appearance of a band at 565 cm^{-1} for Fe-O. The other studies [32,48] also reported a band below 594 cm^{-1} that indicated Fe-O (see Fig. 5B).

The FTIR spectrum of the synthesized IONPs shows a characteristic Fe–O stretching vibration near ~585 cm^{-1} , consistent with iron oxide formation. However, FTIR alone cannot reliably distinguish between magnetite (Fe_3O_4) and maghemite (γ Fe_2O_3) due to overlapping vibrational bands in the 500–600 cm^{-1} region. Meanwhile, Raman spectroscopy analysis can distinguish between magnetite (Fe_3O_4) and maghemite (γ Fe_2O_3). For example, the magnetite has three vibrational bands at 310, 540, and 670 cm^{-1} , while the maghemite commonly shows bands 350, 512, and 720 cm^{-1} [49].

Moreover, a group of researchers was able to prepare IONPs at 80°C with the addition of 25% ammonia and an aqueous extract of *Wormwood* used as a reducing agent. Their consequences were similar to our findings, as the FTIR spectrum of IONPs showed strong peaks recorded between 601 cm^{-1} and 435 cm^{-1} , which relate to the vibration of the (Fe-O stretching) group, confirming successful preparation [10].

The results showed that the absorption bands of the *Wormwood* extract at 1467 and 1170 cm^{-1} (attributed to aromatic stretching and ether group (C-O-C), respectively) were significantly decreased to 1433 cm^{-1} and 1071 cm^{-1} after its use as a functionalized ligand for IONPs, confirming that the organic molecules of the *Wormwood* extract are successfully bound to the surface of IONPs.

Even with the difference in the extract, similar results were observed in previous studies [50] regarding the appearance of the absorption spectrum of the Fe-O bond. The IR results of iron oxide functionalized by Lagenaria siceraria leaf extract showed an absorption peak roughly at 583 cm^{-1} , attributed to the Fe-O bond as reported in literature [39]. This peak, compared to our study, is considered very close.

Iron oxide nanoparticles are created through a series of steps: chelation, redox reduction, hydroxide nucleation, and phytochemical capping. Initially, Fe^{3+} ions from $FeCl_3$ interact with the phenolic and carbonyl oxygen atoms present in *Wormwood* extract phytochemicals. Subsequently, polyphenolic compounds reduce Fe^{3+} to Fe^{2+}, oxidizing phenolic groups into quinone structures. As the pH increases, Fe^{2+} and Fe^{3+} ions undergo hydrolysis, resulting in the formation of mixed iron hydroxide nuclei. These nuclei then dehydrate and convert into iron oxide (Fe_3O_4/γ-Fe_2O_3) nanoparticles. Finally, remaining flavonoids and ether-containing compounds attach to the nanoparticle surface via Fe–O coordination and hydrogen bonding, functioning as capping and stabilizing agents. Shifts observed in the FTIR peaks corresponding to –OH, C═O, C–O–C, and aromatic C═C bonds indicate the presence of these interactions. Furthermore, the Fe–O vibration at 585 cm^{-1} provides evidence for the formation of nanoparticles [51].

3.1.6. Zeta potential results of IONPs

To determine the stability and charge of IONPs in solution, zeta analysis was conducted. The results showed that the IONPs were positively charged, and their zeta potential value was 44.32 mV, as illustrated in Figure S1. The presence of active groups of the *Wormwood leaf* extract contributes to the stabilization and coating of IONPs. It is important to consider the pH value, which affects the sign of the zeta potential. For instance, the surface of nanoparticles can be charged positively or negatively depending on the pH level. Thus, electrostatic repulsion forces between particles enable the stabilization of particles in water. In this regard, as the pH reduces, the zeta potential value increases and becomes more positive, as noted in previous studies [52,53].

In our results, the zeta potential indicates a very high positive value,

which indicates the good stability of dispersed IONPs and confirms that the bonds on the NPs surface are mostly positive. It was previously reported that IONPs obtained high positive values for the zeta potential using various plants, and that positive value for stability was close to our results [38,54]. In the same context, IONPs are prepared using Amaranthus spinosus leaf extract at pH 6. The results of the zeta potential showed a very high positive value reaching 71 mV. They mentioned that this high stability is due to the influence of functional groups in the plant [55]. Regardless of the sign (whether positive or negative), a higher zeta potential value indicates that the particles tend to repel each other and prevent the agglomeration of NPs. In addition, the high electrostatic repulsion force may aid in the long-term stability of NPs in solution. It has been reported that the + 30 mV zeta potential value reflects the stability of the NPs, which may be due to the strong electrostatic repulsive forces present between the NPs [56].

The relatively high positive zeta potential (+44.32 mV) observed in the environmentally friendly manufactured iron oxide nanoparticles can be explained by the combined contributions of the iron oxide's surface chemistry and the pH-dependent ionization state of the phytochemicals in Artemisia absinthium. Although Artemisia extract contains anionic functional groups such as carboxylates and phenols, these groups may be partially ionized under manufacturing and dispersion conditions, thus reducing their negative contribution to the surface charge. This finding consist with the last study that showed green-synthesized IONPs using Ceratonia siliqua L. aqueous extract with a positive charge (+41 mV) [33].

Reports concerning iron oxide nanoparticles manufactured using plant extracts indicate that surface charge values can be positive and are influenced by the functional groups derived from the extract and the pH of the synthesis [57].

In addition, it is illustrated that IONPs possess surface hydroxyl groups that can be protonated under appropriate pH, leading to a positive surface charge [4].

Furthermore, *Wormwood* extract contains nitrogenous biomolecules (such as alkaloids and amine-derived compounds), whose amine groups ($-NH_3^+$) may ionize in aqueous environments, adding an extra positive charge to the surface of the nanoparticles. The synergistic effect of the ionizing surface hydroxyl groups of iron oxide and the ionizing amine functions is expected to explain the observed high positive zeta potential [58]. IONPs prepared with *Wormwood* aqueous extract are an excellent choice for use in a variety of biomedical applications.

3.1.7. Dynamic light scattering (DLS) results of IONPs

DLS was performed in this study to evaluate the size and size distribution of the nanoparticles. It is well known that the poly-disperse NPs solution is unstable and tends to agglomerate over time. The Brownian motion of the NPs enhances colloidal system stability by preventing precipitation and avoiding agglomeration. This motion improves as the particle size decreases [33].

Herein, the DLS size distribution graph of IONPs is shown in Fig. 6. The DLS result shows that the size distribution range of IONPs is (33 ± 2.5 nm) and Polydispersity Index value (PDI) (the square of the standard deviation divided by the square of the mean particle size [59] was = $(8\ /29.7)^2 = 0.07$, indicating monodisperse colloidal system in solution and reflects a narrow, intensity-weighted particle size distribution with good stability, the particles are very closely spaced in size, conforming excellent control over preparation conditions. As expected, the DLS sizes are larger than those reported by TEM. This is because in DLS, the hydrodynamic radius of both the nanoparticles and any adsorbed molecules on the surface of the NPs, such as chemicals in the *Wormwood* leaf extract, is calculated. For this reason, the particle size appears to be higher in DLS compared to TEM results, which is consistent with what was previously explained [60,61].

It was previously mentioned that in DLS, the hydrodynamic radius must be taken into account; it should be larger than the TEM results [62]. In addition, temperature has a significant effect on the DLS results.

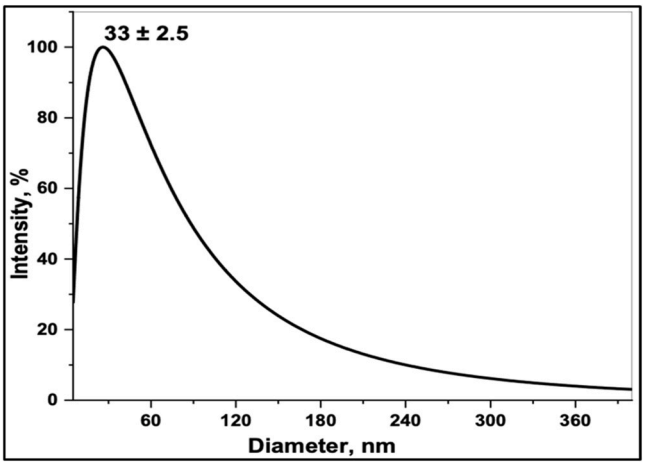

Fig. 6. DLS results of IONPs stabilized by *Wormwood* leaf extract, where a monodisperse colloidal dispersion with a small size (33 ± 2.5 nm) is produced, with a PDI value of 0.06, conforming mono dispersed NPs.

In our study, IONPs were prepared at room temperature, and the size of the produced IONPs was very small, 33 nm, compared to previous literature [63]. It was reported that the particle size of IONPs increased from 464 nm to 1577 nm when the temperature rose from 700°C to 900°C, where the aggregation of iron oxide nanoparticles occurred [63].

3.1.8. Transmission electron microscopy (TEM) results of IONPs

Due to the insufficient accuracy of DLS for such small sizes [64], TEM is used to evaluate the morphological structures and size of IONPs. Fig. 7A shows that the produced IONPs were in the nano size range, with an average size of 17 ± 7.4 nm. The TEM images indicated that the IONPs were monodispersed and well-separated from each other, exhibiting a spherical shape, which is consistent with what was reported in the previous literature [62]. Fig. 7B shows the particle size histogram of IONPs. The Selected Area Electron Diffraction (SAED) pattern of IONPs, which identifies the crystalline structure of materials, is shown in Fig. 7C. SEAD exhibited annular diffraction patterns, confirming its polycrystalline nature, which in turn confirms the presence of randomly oriented crystalline grains separated by granular boundaries. Similar results are shown in the latest study [65]. The presence of polycrystalline domains supports the larger crystallite size obtained from XRD, likely because of nanoparticle aggregation and crystallite coalescence during storage. Specifically, the diffraction rings are attributed to the (220), (311), (400), (422), (511), and (440) lattice planes, which are the most intense reflections typically recorded for spinel iron oxides. The presence of the strong (311) ring, in particular, is characteristic of the magnetite/ maghemite phases. The absence of additional diffraction spots or rings associated with secondary iron oxide phases (such as hematite, α-Fe_2O_3) [66] confirms the purity of the manufactured nanoparticle phase. This SAED pattern is in strong agreement with the XRD results, which exhibits concentric diffraction rings indexed to the (220), (311), (400), (422), (511), and (440) planes corresponding to 0.296 nm, 0.253, 0.210, 0.171, 0.161 nm, and 0.148 nm respectively, of spinel iron oxide (see Table 2). It can be seen that the measured lattice spacing is 0.25 nm, which corresponds to the (311) plane of the Fe_3O_4 crystalline phase, which totally agrees with our findings [67].

The overlap between the dominant XRD reflections, particularly the (400) and (511) planes, and the corresponding SAED rings confirms that both techniques reveal the same crystalline phase. The strong (311)/ (222) related reflections further serve as a fingerprint of spinel iron oxide structures.

The ring-like SAED pattern, rather than discrete spots, further suggests that the nanoparticles are composed of multiple nanosized crystalline domains with random orientations, consistent with TEM

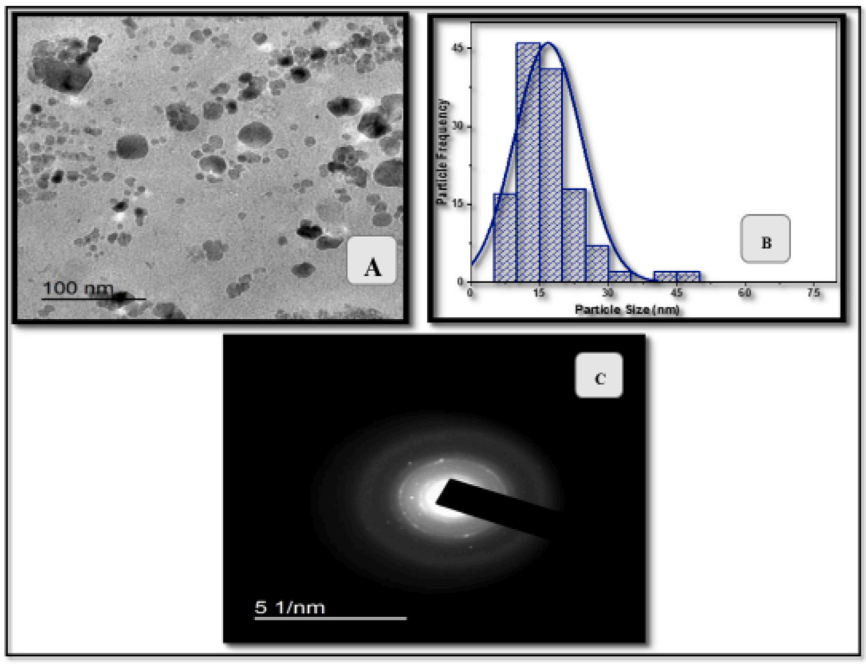

Fig. 7. TEM image of IONPs with nano size (A), particle size histogram (B), and SAED pattern (C).

Table 2
Calculated D-spacings using ImageJ software and their comparison with standard values reported for cubic spinel iron oxide. The experimental D-spacing values displayed good agreement with the theoretical D-spacings.

Plane (*hkl*)	The D-spacing values (nm)
(220)	0.296
(311)	0.253
(400)	0.210
(422)	0.171
(511)	0.161
(440)	0.148

observations. This polycrystalline structure supports the XRD results and describes the larger crystallite size valued by the Debye–Scherrer equation, which may arise from coherent diffraction of aggregated or partially fused crystallites formed during storage.

It is well mentioned that the IONPs obtained a spherical shape after using *Artemisia* (*Wormwood*) leaf extract as a reducing and coating agent, where the size range was between 2.9 and 3.1 nm. However, their stability was lower than our findings [10]. The aspherical IONPs also prepared by using Artemisia vulgaris (*Wormwood*) leaf extract, exhibited sizes in the range of less than 30 nm [18]. The reason for the good stability of current IONPs may be due to the ability of active functional groups in the *Wormwood* leaf extract to fully reduce Fe^{+3} to Fe^{+2} (NPs), as well as the high affinity between the extract and the surface of IONPs. The absence of precipitation and no color change were noted when the IONPs were kept at R.T., in a dry place, and avoiding direct sunlight.

Additionally, when using different plant extracts, spherical shapes of IONPs are produced. For example, IONPs prepared with Plantago major leaf extract showed that the IONPs were spherical and had diameters ranging from 4.6 nm to 30.6 nm [39].

Moreover, Amaranthus spinosus extract produced IONPs with a spherical shape and a diameter of 125 nm [55]. Furthermore, a study reported that stinging nettle leaf extract was used to prepare IONPs, and the TEM results indicated a spherical shape with sizes ranging from 21 nm to 71 nm [38]. In contrast, IONPs were prepared in other shapes that do not align with our results, such as cubic and wire shapes. For example, IONPs were prepared by thermal decomposition, which showed cubic crystals, based on the TEM results. It was reported that the differences may be due to the reaction time or the solvent used in preparing the nanoparticles [68].

Comparing our results with those of a researcher, who prepared Fe_3O_4 nanoparticles with *Wormwood* extract at 75 °C, the researcher obtained a larger average size than our results, ranging from 19 nm to 24 nm. The obtained magnetite nanoparticles were cubic, which is inconsistent with the results of our study [32].

Among the possible shapes of IONPs, it was able to prepare IONPs using B-flabellifer seeds to create hexagonal IONPs, which were well distributed with slight clustering and had a crystal size of 35 nm [21]. Different shapes of IONPs can be produced based on the extract type. For example, a recent eco-friendly study revealed that IONPs synthesized using orange peel extract have a cubic crystalline nanostructure, which is not consistent with our findings [69].

There are other metallic nanoparticles (MNPs) that exhibit a spherical shape when using aqueous *Wormwood* leaf extract as a functionalizing agent in their preparation, such as silver nanoparticles (AgNPs). It was reported that TEM images showed that most of the AgNPs were round in shape and multi-dispersed [70]. In another study, AgNPs reduced by *Wormwood* aqueous extract were mostly spherical and uniform in size, ranging from 30 nm to 50 nm [71]. Our study showed that IONP particles were well dispersed in water, unlike zinc nanoparticles (ZnNPs) prepared by *Wormwood* aqueous extract, which were aggregated and not fully dispersed. The TEM image of ZnNPs indicated that they ranged from spherical to rod-like and plate-like structures [72]. Moreover, copper nanoparticles (CuNPs) prepared by *Wormwood* extract were spherical in shape and approximately small in size (35 nm) [73]. *Wormwood* was used to synthesize nickel oxide nanoparticles (NiONPs), where the results showed that pure nickel nanoparticles were cubic with an average size ranging from 7.49 nm to 10.7 nm [74]. The difference in shape between iron nanoparticles may be attributed to the strength of the phytochemicals used as reducing and covering agents, the pH, or other factors [75].

The DLS and TEM are common devices used to measure the sizes of NPs; however, the sizes of nanoparticles measured by DLS results are usually larger than those measured by TEM. In some cases, this difference has been reported to be between 200% and 300%, raising questions

about the optimal size measurement results. The reason for this difference is that DLS measures the hydrodynamic size, which includes the particle itself as well as any surrounding solvent molecules, whereas TEM measures the core size of the nanoparticle in a solid, dry state. The sample is dried on a copper grid in the case of the TEM technique, and changes in nanoparticle sizes may occur as a result of solvent evaporation [76].

3.1.9. Ultraviolet visible spectroscopy (UV-Vis) results of the colloidal IONPs

The stability of prepared biocompatible IONPs dispersed in water was monitored by UV-Vis for approximately 26 weeks of storage under normal laboratory conditions (25°C), where the samples were kept in a dry, dark place. UV-Vis measurements were performed weekly until the eighth week; after that, they were taken every two weeks. The measurements were repeated three times for more accuracy (see Fig. 8 and Table S1). The samples of IONPs were analyzed at the initial time (fresh preparation), then once a week, with the measurements continuing until 26 weeks after synthesis. A shift in the maximum absorption peak (λ_{max}) of current IONPs was observed throughout the storage period, which reduces the stability of IONPs over time, as reported in previous studies [77]. Observations of IONPs in this study also exhibited that the color of IONPs was changed slightly, becoming darker after more than 18 weeks in comparison to the freshly produced IONPs, confirming that the stability and size of colloidal IONPs change over time, based on what is mentioned in similar literature [77]. According to a previous study, the position of the maximum absorption determined using UV-Vis depends on numerous factors, including the shape, solvent, dielectric constant, and size of the nanoparticles [78,79]. In our study, all UV-Vis peaks confirmed the formation of IONPs, with the peaks being centered at 295 nm (at the initial time) and at 298 nm after 26 weeks (see Fig. 8, Table S1). This completely agrees with the study that presented the UV-Vis results of IONPs, which showed an absorption peak at 295 nm [77,80]. The λ_{max} of *Wormwood* leaf extract was centered in the range of 340–430 nm, confirming its non-interaction with the IONPs region.

Another study supports the full consistency with our results, as the researcher obtained IONPs from the extract of Senna bicapsularis, where the typical absorption peak at 295 nm confirmed the occurrence of IONPs [77]. Even when using different plant extracts in the preparation of IONPs, the results were similar to our findings. For example, a study reported that IONPs functionalized by Amaranthus spinosus leaf extract showed UV results confirming that the absorption peak of IONPs appeared at 290 nm, thereby confirming the successful formation [55].

In contrast to our results, the highest SPR peak was located at 285 in a study in which IONPs were prepared by Orange Peel extract [69]. Additionally, it has been reported that IONPs were synthesized by Saccharum arundinaceum extract, which serves as a capping and reducing agent. The results displayed that the SPR at 370 nm for IONPs was not quite consistent with our results [13].

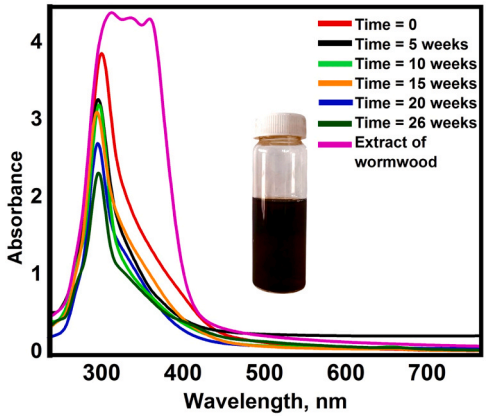

Fig. 8. UV-Vis spectra of the extract of *Wormwood*, as well as the stability of IONPs over 26 weeks.

It is demonstrated that careful selection of ligands is very significant for the function and stability of nanoparticles, as these ligands are responsible for the final sizes and shapes of nanoparticles. Furthermore, in our study, the production of iron oxide nanoparticles using *Wormwood* extract took a shorter time (less than half an hour), possibly due to the ability of the plant's organic compounds and their robust chemical structures to reduce the precursor material into NPs [10].

According to previous studies, the functional groups of functionalized ligands contribute significantly to controlling the shape, stability, and size of nanoparticles. Similarly, it was established that the ligands containing carboxyl (COO^-), hydroxyl (OH), and carbonyl (-C═O) groups in their structure provide a strong stabilizing effect on nanoparticles [81,82]. From these results, we confirm the successful preparation of IONPs when prepared by *Wormwood* extract, which contains the same functional groups.

Different storage times (from 0 to 26 weeks) of IONPs resulted in absorption peaks at different wavelengths (295, 296, 297, 297, 298, and 299 nm), which seem to be lower than the absorption peak of the extract of *Wormwood*. The SPR of *Wormwood* leaf extract, as a stabilized ligand of IONPs, is shown as a purple curve for comparison with IONPs. The absorption peaks of the extract at 280–400 nm indicate the presence of flavonoids, alkaloids, and phenolic acids. The broad peak from 280 to 290 nm indicated $\pi \rightarrow \pi^*$ transitions of aromatic rings (phenolics) [83], while at 320–360 nm, attributed to $n \rightarrow \pi^*$ transitions of carbonyl group (C═O groups) in the flavonoids [84]. The disappearance of some peaks of the extract confirms the success of those groups in reducing Fe^{+3}, producing IONPs with high stability.

From Table S1, it can be observed that the position of SPR gradually increased starting from the third week until the twelfth week. After that, the SPR decreased slightly, but its intensity decreased with a broad peak, indicating the production of different sizes. This changing behavior could be attributed to the storage of IONPs over time. In addition, the absorption intensity of IONPs changes significantly with particle size. We observed that an increase in the absorption band occurred as the particle size increased. This is due to the tendency of the IONPs to agglomerate or aggregate over time. These findings are in line with the literature [85–87].

Furthermore, the SRP bands are generally used in determining the sizes of metal nanoparticles (MNPs) as investigated by the literature [88], where larger sizes are produced when SPR shows a redshift in UV-Vis results, which totally agrees with our findings.

3.2. Stability study of IONPs

Phytochemicals, including flavonoids, polyphenols, terpenoids, and other organic compounds, link to the surface of nanoparticles by coordination and hydrogen bonding to function as both reducing and capping agents in plant-mediated synthesis. Nevertheless, compared to covalent surface functionalization, the interactions, such as physical adsorption, hydrogen bonds, and coordinate bonds, are rather weak. Adsorbed biomolecules may desorb over time, organic fragments may break down, and interactions with light, water, and air may change capping. As a result, there is less surface protection, which makes it possible for nanoparticles to cling to one another. This is one of the primary causes of the gradual aggregation and loss of colloidal stability of green-synthesized particles [89,90].

Even at room temperature, Fe_3O_4 nanoparticles are susceptible to oxidation in air. Surface Fe^{2+} ions oxidize to Fe^{3+}, causing a topotactic transition toward maghemite (γ-Fe_2O_3). As the Fe^{2+} / Fe^{3+} ratio fluctuates with aging, this continuous oxidation and phase transition have a substantial impact on magnetic characteristics and nanoparticle stability [91].

3.2.1. Effect of pH on the stability of IONPs

Acidic or basic conditions can control the change in the size of nanoparticles, and in addition to altering their shape [25,92]. They may affect surface interactions, leading to the formation of aggregates or the disintegration of particles. Nanoparticles may interact with solution components such as ions or other molecules, resulting in a change in their optical and chemical properties. These interactions can also affect the stability and distribution of nanoparticles [25]. Additionally, an increase or decrease in the pH value can influence the surface charges of nanoparticles, affecting their electrical behavior and interactions with other molecules. Certain types of nanoparticles may become more toxic under specific conditions, impacting their use in medical or environmental applications [93]. The pH level is crucial and can affect the chemical composition of nanoparticles. For instance, some metal nanoparticles can oxidize in an acidic environment, whereas they can react with bases and produce side products. It is worth noting that some nanoparticles may lose their magnetic properties in either acidic or basic environments [94].

The results of this study indicate the stability of IONPs prepared by *Wormwood* leaf extract at pH 7.6. The pH of the *Wormwood* leaf extract solution was 4.2, and after it was added to the $FeCl_3.6\ H_2O$ solution, stirring was sustained until the pH stabilized at 7.6, confirming the successful preparation of IONPs, where the color of the solution was blackish brown, and the SPR value was centered at 295 nm, as shown in Fig. 9A. This is SPR consistent with some previous literature [77,80]. This stability persisted for more than six months. The reason for this good stability is attributed to the abundance of functional groups (carbonyl and hydroxyl) present on the surface of IONPs. With time, the SPR value decreased slightly, suggesting the aggregation of the produced IONPs. Furthermore, the stability of IONPs was investigated at low pH using hydrochloric acid (HCl) (0.1 M). The intensity of 3.7, 3.6, 2.4, 2.1, and 1.4 was observed at pH 7.6, 6.5, 4.7, 3.2, and 2.3, respectively (see Fig. 9A). The lowest value of the intensity occurred at the very lowest pH (pH 2.3), indicating aggregation of IONPs. As the pH value decreased, a color change occurred, shifting from dark brown to brown (see Fig. 9A). This was also followed by a change in the SPR value, which is consistent with the previous study [43].

The SPR shift from high to lower wavelengths (blue shift) and broadening of the peak were observed as HCl amounts were increased (5–25 μL), indicating different sizes of IONPs were produced (Fig. 10 A). A related study showed that changing the pH to get a shorter wavelength altered the IONPs particles' SPR absorption intensity [13]. Therefore, the manufacture homogeneous NPs with adjustable sizes is one of the major problems in the field of nanoscience and nanotechnology. Based to the later study [95,96], many properties of magnetic nanoparticles were size-dependent. For instance, the magnetic nanoparticles become superparamagnetic when their size is below 10 nm [95,96].

Notably, the best result of IONPs was at pH 7.6, because the stability is very high. While the pH of colloidal IONPs decreased to less than 6, the intensity of UV-Vis peaks was reduced, and twists occurred, confirming low stability and polydispersity. The high stability of IONPs may be attributed to the fact that at pH 7.6, the electrical charges of the biomolecules and the coating agents did not change, preserving their ability to bind and reduce iron ions. This finding is consistent with the previous studies [33].

Higher pH values were also studied by gradually increasing the IONPs colloidal solution using sodium hydroxide (NaOH, 5–25 μL) (0.1 M) (see Fig. 9B). As the pH value increases, the color changes and becomes blacker, as shown in Fig. 9B. Additionally, a change in the intensity of 3.6, 3.8, 4, 4.1, 4.4 was observed at pH 7.6, 8.1, 8.9, and 9.1, and 10.5, respectively as shown in Fig. 10B, with a shift noted at higher wavelengths (redshift), confirming the increased size of the NPs. It is important to mention that the nano-solution loses its super magnetic property due to the occurrence of aggregation at a high pH, which is attributed to the increase in deprotonated carboxyl groups (OH^-) on its surface [97,98].

For example, as indicated by stability experiments in aqueous media, nanocrystals (iron oxide nanocrystals and titanium oxide) exhibit much interaction between several factors: a pH-dependent type of charge on the surface and pH-dependent deprotonation of the ligand. Moreover, minor modifications to the structure of ligands can lead to changes in the solubility of these ligands and thus increase their binding affinity. However, the binding group remains, and the colloidal stability property is able to extend to include other ligands, such as carboxylate head groups, phosphonate, and catechols. Therefore, the colloidal stability map can be used to predict which ligands will offer colloidal stability at a given pH value [93].

The form and height of the SPR bands alter as the pH level changes. On the other hand, the absorption peaks of IONPs gradually increased with increasing pH, indicating that they underwent a redshift, which is due to the increase in the average size of the metal nanoparticles as noticed in the literature [13].

We have demonstrated that IONPs can respond to changes in pH, acidity, and cluster formation. When the pH of the surrounding environment is low or high, the attraction and repulsion between particles play a vital role in the pH-responsive behavior of particles. Because the different electrostatic interaction behaviors of particles at varying pH values are not caused by a chemical change but by simple differences in

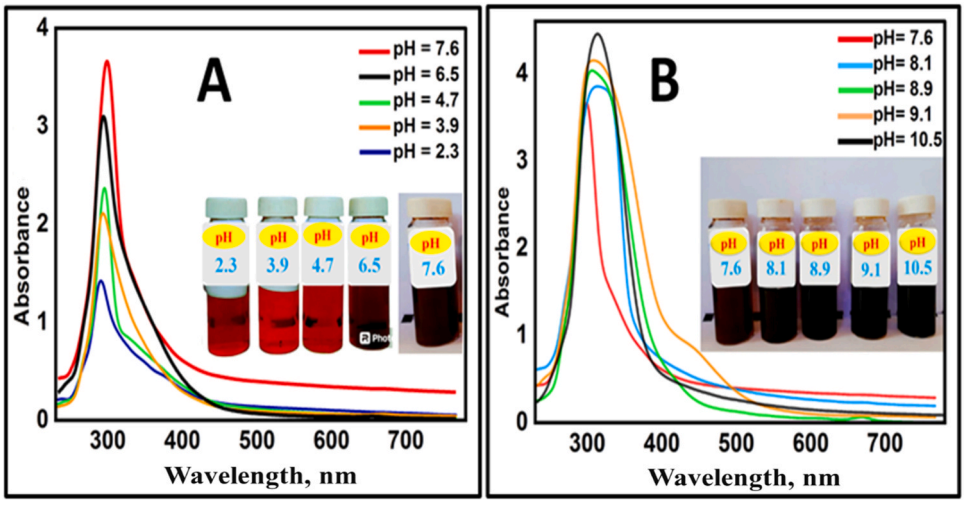

Fig. 9. UV-Vis spectra of IONPs at different pH values formed by adding HCl (0.1 M) (A) and NaOH (0.1 M) (B) to dispersed IONPs stabilized by *Wormwood* leaf extract.

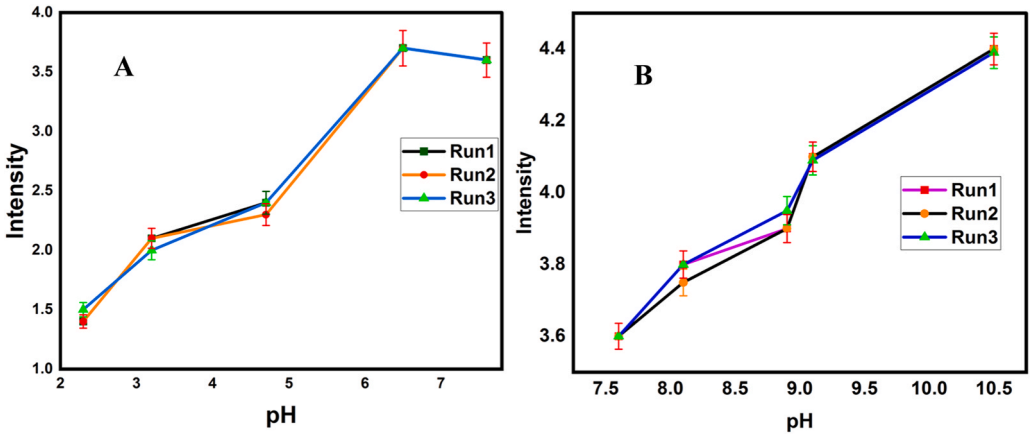

Fig. 10. (A) Intensity plot of IONPs versus the pH. The values show the mean ± standard deviation of three measurements in acidic conditions. (B) Intensity of IONPs versus the pH range from 7.6 to 10.5 under basic conditions. Data is shown as mean ± standard deviation. Every sample was performed in triplicates in basic conditions.

protons, as reported [98]. The consequences of the current work indicate that the optimal stability of IONPs prepared by *Wormwood* leaf extract should not be higher than pH 9.3 and not lower than pH 6.8 to avoid aggregation and loss of magnetic properties. The study [94] confirmed that magnetic properties were present at pH 6.5 and 7.5 and were lost at higher pH levels.

In addition, it was mentioned that changing the medium solution to include alkaline amines would be able to enhance the magnetic properties of IONPs and reduce their particle sizes, which addresses the challenge of maintaining magnetic performance at smaller sizes [99].

The effects of pH values (1.2, 7.5, and 12.5) and washing solvents on the magnetic characteristics of the NPs were also investigated in a different study that described the green method of creating green nanomagnetic iron oxide particles (GNMIOPs). The results demonstrate that numerous GNMIOP features are significantly impacted by both pH levels and washing procedures. For instance, the highest saturation magnetism experiment in GNMIOPs was prepared at pH 7.5 and 12.5 [100].

It is very rare to find previous studies concerned with the stability of nanoparticles over long periods of time. For example, Park et al. [101]. proposed that the stability of iron oxide nanoparticles coated with citric acid was experimentally verified under different pH values (pH 5, 7, 9, 11). It demonstrated that the stability and dispersion of IONPs did not last beyond 30 days. Aggregation occurred at pH 11 due to the adsorption of citric acid on the NPs' surface. That study did not even achieve the level of stability obtained in our study [101].

Similarly, another study showed that the initial colloidal stability of IONPs lasts for more than three months, depending on the storage method and period, which affects the toxicity of IONPs. Additionally, adding numerous charged groups such as polyethylene glycol (PEG) to the IONPs surface enhances the stability of NPs by combining charge-charge repulsion with steric hindrance [102]. It was also reported that IONPs are synthesized by the co-precipitation method, one of the most common methods for synthesizing magnetic IONPs. The results exhibited that the NPs were stable, with all nanoparticles being highly stable and showing no signs of agglomeration over 168 h (one week) [103], which is a much shorter stability time compared to the high stability achieved in this study. Thus, it can be considered that the *Wormwood* leaf extract is a good choice for synthesizing highly stable IONPs because its chemical structure contains multiple active functional groups.

It is well mentioned that pH controls the Fe3+ hydrolysis. Ions remain dissolved at low pH, hydroxide nuclei are formed at neutral pH, and rapid precipitation takes place at higher pH values.

At low pH : $Fe^{3+} + H_2O \rightleftharpoons Fe(H_2O)_6^{3+}$

As pH increases:

$Fe^{3+} + OH^- \rightarrow Fe(OH)^{2+}$

$Fe^{3+} + 3OH^- \rightarrow Fe(OH)_3\downarrow$

Further, pH controls reduction by flavonoids, where higher pH favors a higher reduction rate and higher nucleation rate. Phenolic groups reduce Fe3 + only when deprotonated, and this deprotonated phenolate is a stronger electron donor and stronger Fe chelator.

$Ar–OH \rightleftharpoons Ar–O^- + H^+$Additionally, pH controls surface charge & stability. At higher pH, more Fe – O^- are formed ($Fe–OH \rightleftharpoons Fe–O^- + H^+$) which results in higher zeta potential and better dispersion. Whereas at lower pH, aggregation is favored due to the positive surface of $Fe–OH_2^+$. Fe^{2+} and Fe^{3+} ions cannot completely precipitate in an acidic environment due to a lack of OH^- ions. Instead of magnetite, this could result in the development of alternative iron oxide phases, including hematite or goethite (FeO(OH)). Low pH nanoparticles typically have bigger particle sizes, poor crystallinity because of incomplete reactions, increased agglomeration because of delayed nucleation, and inadequate surface charge for electrostatic repulsion [104].

Ferrous hydroxide ($Fe(OH)_2$) and ferric hydroxide ($Fe(OH)_3$) can form in large quantities when the pH of the precipitate is excessively high due to excess OH^- ions. Agglomeration or the creation of nonmagnetic phases may follow from this. Additionally, uncontrolled nucleation brought on by a higher pH can produce polydispersity and less homogeneous nanoparticles [105].

3.2.2. *Effect of temperature*

Time, temperature, and pH changes can affect the stability and size of iron oxide nanoparticles as mentioned above. It has been reported in some studies that high temperatures can accelerate the aggregation processes, while low temperatures can delay them [43]. In this study, IONPs are prepared by *Wormwood* leaf extract at room temperature (R. T.), which could produce small-sized IONPs with great stability. Since temperature has an important influence on IONPs activation, the effect of different temperatures on the synthesized IONPs was studied at R.T., 40 °C, 60 °C, and 90 °C, as shown in Fig. 11.

Herein, a series of experiments was conducted, and the changes in the SPR peak were monitored using UV-Vis device. The samples were prepared at varied temperatures, as illustrated in Fig. 11. At room temperature, the sharp SPR of iron oxide nanoparticles was 295 nm, indicating good stability.

IONPs are heavily temperature dependent; for instance, the SPR peaks change and decrease regularly from 295 nm to 292 nm, 291 nm, and 289 nm when the temperature increases from 25°C to 40°C, 60°C,

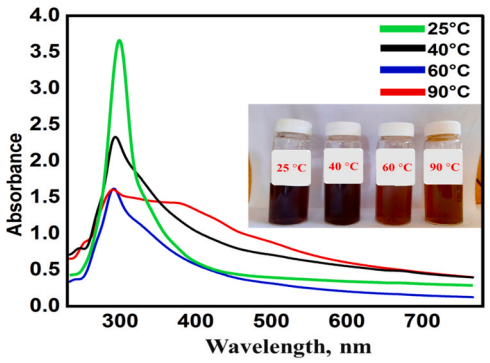

Fig. 11. Variation of Absorbance with Wavelength at different temperatures.

and 90°C, respectively. There is a noticeable change in the absorption width, as well as the color change, as it turns dark brown after being black. These changes are completely identical to a previous study in which Aloe vera extract was used in the preparation of IONPs [43].

According to the literature, the adsorption capacity of IONPs at a higher temperature (90 °C) is 5 times higher than at a lower temperature (25 °C), which has direct applications in the separation of different metals from their solution form [24]. It is also reported in the literature that IONPs are spherical at lower temperatures but have a nanorod structure at a higher temperature (90°C) [104].

The SPR bands of IONPs shift towards a higher wavelength, and the absorption range becomes wider with increasing temperature. Similar investigations of green-synthesized IONPs were noted in the literature [13]. The UV-Visible results showed a sharp peak for IONPs at room temperature. However, at 90°C, the surface decomposition rate of IONPs is larger and wider than at room temperature, with a new peak occurring at roughly 410 nm, confirming that an aggregation process has happened. Furthermore, at 40°C and 60°C, the wavelength width of IONPs also increases significantly, confirming the occurrence of agglomeration (see Figs. 11 and 12).

Moreover, there are no notable alterations in the SPR position or absorption width from 40°C to 60°C. However, at 60°C and 90°C, a remarkable difference between them is observed in the SPR position of IONPs. Increasing the temperature also negatively impacts the stability of the nanoparticles, size, size distribution, and the formation of larger clusters, due to the loss of charge on the surface of IONPs [63]. It has also previously been mentioned that the particle size of IONPs increased with rising synthesis temperatures between 40°C and 60°C [106]. Using other extracts, it was reported that iron oxide nanoparticles were synthesized

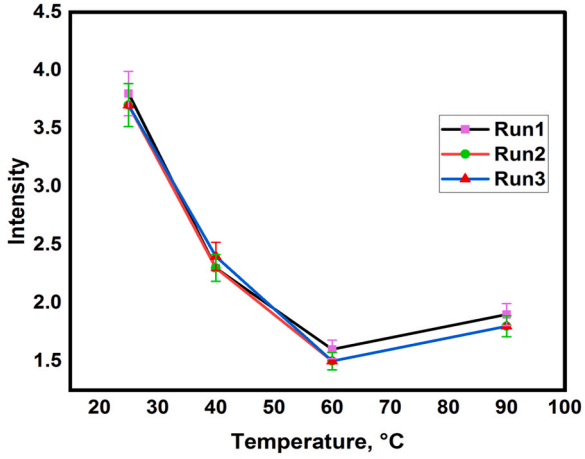

Fig. 12. Intensity of IONPs versus the temperature range from 25°C to 90°C. Data is shown as mean ± standard deviation. Every sample was carried out in triplicate.

using Aloe vera extract, at different temperature conditions of 25°C and 90°C. The study indicated that with increasing temperature, the size of nanoparticles increases [24].

Furthermore, it was reported that iron oxide nanoparticles were synthesized at different temperatures, 190°C, 220°C, and 235°C, using continuous growth methods. The study confirmed that increasing the temperature leads to reduced stability and formation of larger nanoparticle sizes [107]. In addition, Fe_3O_4 nanoparticles exhibited superparamagnetic behavior at room temperature according to the literature [108].

Accordingly, we determined that it is better to prepare iron oxide nanoparticles at room temperature to avoid agglomeration or aggregation.

The structural properties of iron oxide nanoparticles have been found to be strongly influenced by the reaction temperature during synthesis; lower temperatures favor irregular and aggregated particles, while higher temperatures promote well-defined shapes and enhanced crystallinity due to thermally activated crystal growth and recrystallization [109].

Li et al. [110]. showed that great attention could be paid to the particle size and crystalline properties of Fe_3O_4 nanoparticles, which gives their potential applications in the medical and industrial fields. These applications require magnetic particles to have a appropriate size to achieve a good balance between suitable magnetic performance and effective surface area [110].

According to reports, temperature is a crucial factor influencing the size of iron oxide nanoparticles (NPs). As the temperature rises, the oxidation reaction rate and nucleation dynamics alter, which can result in smaller particle sizes early on but also larger distributions at extreme temperatures because of growth mechanisms [111].

So, it is seen that higher thermal energy improves atom mobility → better crystal ordering → smaller but more crystalline particles. Thus, temperature changes the kinetics of hydrolysis, nucleation, growth, crystal ordering, and oxidation.

3.3. *Antioxidant assays*

Antioxidants, as we know, protect cells from the dangerous effects of reactive oxygen species (ROS). Excessive reactive oxygen species lead to oxidative damage to cell components in the bodies of living organisms and promote several diseases, including aging, cancer, atherosclerosis, and malaria [112,113]. In this study, the most common screening method (DPPH assay) was used to conclude the antioxidant capacity of the aqueous extract of the *Wormwood* and IONPs functionalized by the same extract.

3.3.1. *Antioxidant activity test of wormwood extract*

Herein, the antioxidant measurements of *Wormwood* leaf extract were carried out using the DPPH test, and the concentrations of the aqueous *Wormwood* extract used were 200, 300, 400, and 500 µg/mL. When DPPH is added to the last concentrations, a momentary change in color occurs from violet to pale yellow. This pale color and the speed of color change indicate the strength of the compounds found in the aqueous extract to scavenge DPPH free radicals (see Fig. 13). The technique depends on reducing the methanolic DPPH solution in the presence of antioxidants that donate a hydrogen (phenolic compounds and flavonoids in the aqueous extract of *Wormwood*); due to the generation of the non-radical form DPPH-H through the reaction process. This is consistent with a study [114], which indicates that *Wormwood* leaf extract can reduce the stable radical DPPH to the corresponding yellow diphenylpicryl hydrazine. All concentrations in this study displayed antioxidant effects at very high rates (see Table S2 and Fig. 14); the rate varied according to the concentration, and in general, all concentrations had an antioxidant effect very similar to the standard sample (ascorbic acid). However, the best value was at 500 µg/mL (94.2%) as compared with the standard (ascorbic acid) (99.2%).

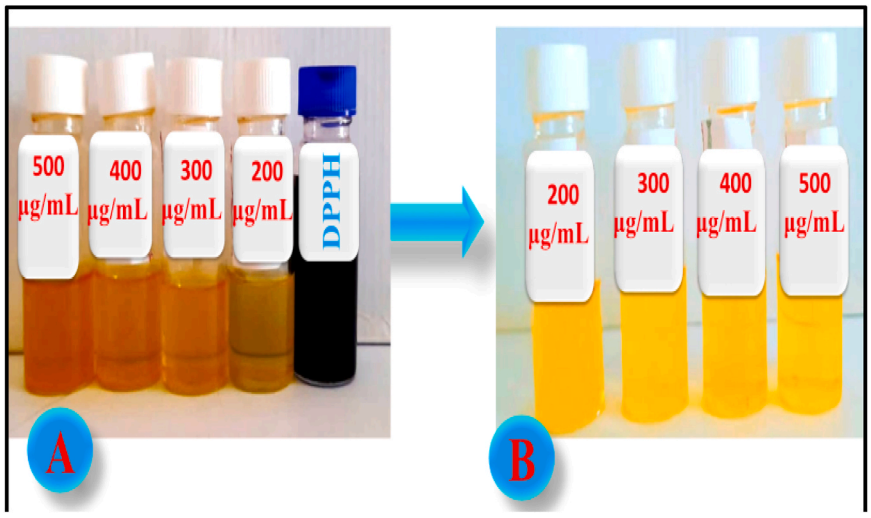

Fig. 13. Illustration of color change: (A)*Wormwood* extract samples before adding DPPH; (B) *Wormwood* extract samples after adding 200 µL of DPPH.

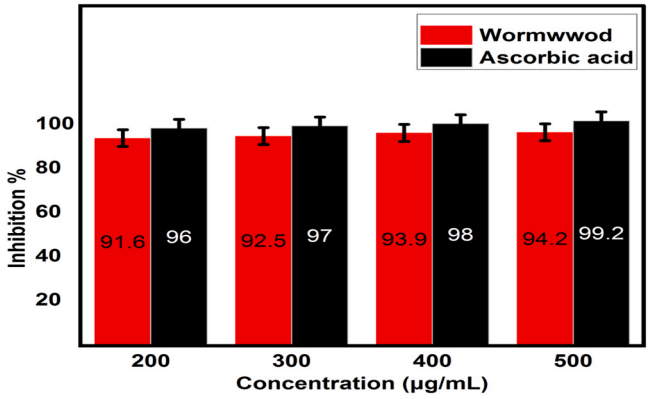

Fig. 14. Variation of the percentage inhibition of DPPH radical with various concentrations, including *Wormwood* and Ascorbic acid. Analysis of variance (ANOVA) was carried out to assess the significance of comparing *Wormwood* extract to the control group. A p-value < 0.0001 was considered statistically significant compared to the control group.

Based on previous research [115], the antioxidant activity of chemical compounds in extracts depends on several factors, including the number of hydroxyl (OH^-) groups directly attached to the aromatic rings and the type of solvent used. A study stated that the aqueous extract of *Wormwood* gave the highest antioxidant activity of 95.56% compared to other solvents, indicating that compounds with strong free radical scavenging ability are highly polar. In addition, recent studies have shown that the whole Artemisia vulgaris Linn plant has polyphenol composition, where its aerial parts, leaf extract, and essential oil have antioxidant properties [115].

In comparison to other studies using higher concentrations than ours, the antioxidant effect was less pronounced. For instance, the high-dose extract of *Wormwood* (100 mg/mL) showed the highest antioxidant activity at 91.1 ± 0.054%, whereas at medium-dose of extract (50 mg/mL) and low-dose (20 mg/mL) the antioxidant activities were 89.6 ± 0.012%, 84.1 ± 0.02%, respectively [116].

Therefore, the antioxidant effects of the aqueous extract used in our study showed high values of antioxidant activity, indicating the superiority of polar solvent extraction (distilled water and ethanol), also due to the extraction method based on the Soxhlet apparatus, as mentioned in the earlier study that utilized the Soxhlet method, where its results are close to our findings [117].

The antioxidant capacity of *Wormwood* extract was tested, and researchers found that many phytochemicals could donate an electron or a hydrogen atom to the DPPH free radical. Different concentrations of *Wormwood* extract (150, 200, 250, and 300 g/mL) were used, and the results ranged from 85.50% to 118.02% [118], compared to our study. The results in this study were higher despite using lower concentrations of *Wormwood* extract. According to these results, we can obviously see that the aqueous extract of *Wormwood* has antioxidant properties and can be used to scavenge free radicals.

3.3.2. *Antioxidant activity test of IONPs*

The antioxidant activity of IONPs with a size of 17 ± 7.4 nm was investigated in this study. The details are shown in Table S3, where very high antioxidant percentages were observed even at low concentrations. The concentration of IONPs functionalized by *Wormwood* leaf extract was 500 µg/mL, and different concentrations from 200 µg/mL to 500 µg/mL were tested as antioxidants. From Table S3, it can be concluded that the antioxidant activity percentage increases with increasing sample concentration (see Table S3 and Fig. 15). In addition, the color change is shown in Figure S2. For example, the antioxidant activity measured by DPPH of IONPs increased in the order of 47.2%, 58.2%, 78.2%, and 88.6% as the concentration of IONPs increased from 200, 300, 400, and 500 µg/mL, respectively. Meanwhile, the inhibition

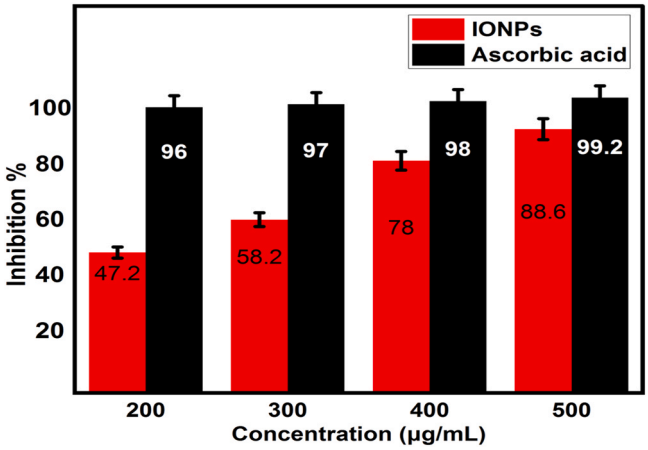

Fig. 15. Variation of the percentage inhibition of DPPH radical with various concentrations, including IONPs and Ascorbic acid. Analysis of variance (ANOVA) was performed to assess the significance of comparing IONPs to the control group. A p-value < 0.0001 was considered statistically significant compared to the control group.

ratio of ascorbic acid increased by 96%, 97%, 98%, and 99.2% at the same concentrations mentioned. Furthermore, the results exhibited a higher scavenging percentage than the findings of previous studies on the same subject [119], indicating that the green-synthesized cationic IONPs interacted with the free radicals of DPPH and displayed radical-scavenging activity, which consists of an electron pair surrounding a nitrogen atom. Thus, iron oxide nanoparticles can be considered an antioxidant. This aligns with a previous report presented in the literature [120].

In general, the evaluation of antioxidants is very valuable for protecting the biological systems from ROS, for example, hydrogen peroxide, hydroxyl radicals, or singlet oxygen in living systems. This is consistent with a study that demonstrated that the increase in antioxidant activity against DPPH radical depends on the concentration of IONPs. It was stated that the external organic layer of nanoparticles is responsible for the highly antioxidant activity of IONPs, which consists of different plant components from (Ficus carica Fruit) FCF extract and enables them to trap ROS, such as superoxide anions, hydroxyl radicals, hydrogen peroxide, etc., on their surface [47].

In addition, the size of NPs and the concentration of ferric chloride have a considerable impact on the antioxidant potential. The study reported that the antioxidant power results in different tests indicated that magnetic iron oxide Fe_3O_4 nanoparticles synthesized from Artemisia extract could be influential natural antioxidants beneficial for maintaining health due to their antioxidant properties in cancer cell lines. The antioxidant effect was evaluated by the DPPH test for magnetite samples, Fe_3O_4, prepared by *Wormwood* extract, where the findings showed the antioxidant measurements of various samples at a variety of concentrations of $FeCl_3$. The sample with the highest concentration of 0.1 M had the best total antioxidant results, within the range of 89.2%, compared to our study. This concentration used is much higher than the concentration applied in our study. It is worth noting that the highest concentration in our study provided a percentage of 88.6% [32].

Moreover, Artemisia extract was used with other nanoparticles. For example, the antioxidant activity of copper nanoparticles (CuNPs) synthesized with Artemisia extract was evaluated by DPPH assay, and different concentrations were used. At 100 μg/mL of Artemisia extract-synthesized copper nanoparticles, the highest antioxidant activity was obtained, reaching 67%, indicating that Artemisia extract is rich in antioxidant compounds [73].

Using various plant extracts, IONPs have demonstrated antioxidant potential; for instance, researchers reported that the antioxidant potential of IONPs synthesized from Amaranthus spinosus leaf extract was investigated by using the DPPH assay. The consequences visibly show that IONPs exhibited a high antioxidant potential of 93%. This may be because of phenolic and amaranthine compounds on their surface, which can scavenge the harmful effects of free radicals [55].

Furthermore, the free radical scavenging capacities of the green-synthesized NPs can be attributed to the presence of bioactive ligands in the extract that exhibit worthy antioxidant activities; thus, the surface-functionalized IONPs by *Wormwood* extract presented significant free radical scavenging activity. According to Sultana et al. [121]. the antioxidant activity increases with increasing concentration, and the results of free radical scavenging activity showed that the antioxidant potential of IONPs depends on the concentration. The DPPH scavenging activity was in the range from 57% to 87% in the case of IONPs, which was relatively lower than that of ascorbic acid as a reference at the same concentration, aligning with our study. Additionally, in a study, the antioxidant activity of IONPs was measured by DPPH assay, where 10 μL of biosynthesized IONPs were mixed with 2.5 mL DPPH solution. The free radical scavenging rate was low at 35.44%, which is due to the low concentration of IONPs used [122].

The strong DPPH radical scavenging activity of the biosynthesized IONPs (up to 88.6%) is primarily attributed to the phytochemicals capped on the surface of the nanoparticle, with a secondary contribution from the iron oxide core itself, which consists with the literature [123].

Phytochemicals on the surface play a primary role. During green synthesis, plant-derived biomolecules such as phenolics, terpenoids, flavonoids, and proteins remain bound to the surface of IONP, as evidenced by FT-IR analysis. These surface capping agents possess hydroxyl and other redox-active functional groups capable of donating hydrogen atoms or electrons to DPPH radicals, resulting in their reduction and discoloration. As the concentration of IONPs increased, the high scavenging efficiency therefore increased, reflecting the synergistic effect of a high surface area and dense coverage of antioxidant phytochemicals on the NPs because of the increase in the extract, which contributed not only to efficient nanoparticle synthesis but also to the enhanced antioxidant activity. This observation aligns with earlier studies reporting similar mechanisms [124].

In the second role, the iron oxide core may contribute indirectly to the antioxidant activity. Fe^{2+}/Fe^{3+} redox couples present on the IONP surface can facilitate electron transfer reactions, enhancing radical quenching under certain conditions. Moreover, the nanoscale size increases surface reactivity, which can promote interaction between DPPH radicals and surface-bound redox centers. However, this contribution is considered supportive rather than dominant, as bare IONPs typically show much lower scavenging activity compared to phytochemically capped ones [125].

It is illustrated that the phytochemicals present in the extract play a remarkable role in scavenging free radicals; thus, these pharmacological properties of phytochemicals improve the therapeutic properties of nanoparticles with better biological activity. The green-functionalized IONPs can be possible candidates in many biomedical applications due to their high cytocompatibility and antioxidant activity [21,73,74].

3.3.3. Antibacterial activities of iron oxide nanoparticles

In this century, antimicrobial resistance is a major threat to global health, as most bacteria acquire multiple antibiotic resistance through exposure to traditional antibiotics. As a result of their inability to selectively target pathogenic bacteria, difficulties in targeting the required place, poor solubility, instability, low bioavailability, and high doses or frequency of dosing are needed to sustain therapeutic plasma concentrations [126,127].

This requires the development of alternative drugs to improve the effectiveness of antimicrobials and reduce the incidence of drug resistance. In this era, nanotechnology has entered the development and manufacture of nanoparticles that can carry out and deliver antibiotics to the target site. Among these nanoparticles, small IONPs with different sizes and shapes are the most widely studied nanomaterials for antibacterial applications, due to their smaller ion particle sizes and higher surface energies [128,129].

3.4. Antibacterial activity

3.4.1. Time-kill curve assay of S. aureus bacteria by IONPs

The time-kill test of IONPs against Gram-positive Staphylococcus aureus was evaluated. The test was performed by suspending the bacterial cell in a medium containing IONPs. *Wormwood* extract was also used at the same basic concentration (0.0035 g/mL) to evaluate the antibacterial activity. The suspension without adding IONPs was also used as a control (Daptomycin 10 μg/mL). The results obtained showed effective antibacterial actions of IONPs against Gram-positive Staphylococcus aureus at different times (0, 1, 2, 3, 4, 5, and 6 h) (see Fig. 16). The concentrations of IONPs used were (10, 40, and 60 μg/mL), where we observed in the first hours a decrease in absorption (λ_{max} 600) with increasing the dosage of IONPs. This decrease was rapid at the highest concentration of 60 μg/mL, compared to the rest of the concentrations. The effect of IONPs is increased from the fourth hour to be quite similar to the control, confirming the good biocompatibility of IONPs. Daptomycin, used as a control at the lowest dose used in this study (10 μg/mL), showed results similar to IONPs at 60 μg/mL, particularly within the initial three hours (from the first hour of incubation to the third

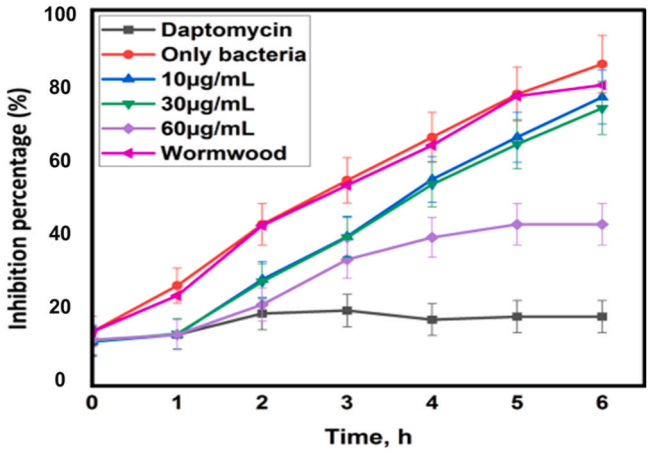

Fig. 16. Variation of inhibition percentage of IONPs with time, including Daptomycin *and S. aureus* bacteria. The bars represent the calculated standard deviations from at least three independent experiments.

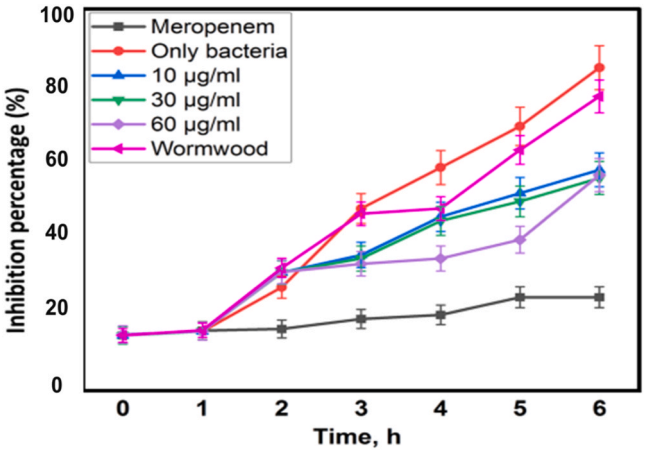

Fig. 17. Variation of inhibition percentage of IONPs with time, including Meropenem and *A. baumannii* bacteria. The bars represent the calculated standard deviations from at least three independent experiments.

hour). It is noteworthy that when used alone, *Wormwood* extract showed very weak antibacterial activities. A previous report indicated that silver nanoparticles had significantly stronger antibacterial effects than the crude extract against all types of bacteria used in the study [130].

In general, the use of aqueous *Wormwood* extracts to synthesize IONPs shows a clear and promising effect in eliminating and destroying the bacterial cell wall, due to the presence of active compounds on the surface of IONPs. They inhibit bacterial proliferation through several simultaneous mechanisms, such as DNA damage, generation of ROS, degradation of critical proteins, and damage to the S. aureus bacterial cell wall, according to the literature [131].

In the same context, cerium oxide nanoparticles showed a clear effect in inhibiting the growth of five types of bacteria, one of which is the Gram-positive Staphylococcus aureus, and the results revealed significant changes in antibacterial activity due to changes in the membrane structure and cell wall composition [132]. For this reason, the nanoparticles prepared in our study might be a good substitute for common traditional antibiotics, resolving global issues, such as bacterial resistance.

The nanotechnology approach is expected to represent a new tool to combat pathogenic bacteria if the concentration is increased beyond the currently used concentrations. In a similar study against the Gram-positive Staphylococcus aureus, CuNPs were used as a therapeutic, and the kinetics of bacterial killing were studied. It was found that the minimum inhibitory concentration values had a lesser effect, while the higher concentration amount showed a significant effect in inhibiting the bacteria [133].

3.4.2. *Time-kill curve assay of A. baumannii bacteria by IONPs*

The results obtained showed effective antibacterial actions against the Gram-negative bacteria *A. baumannii*, which were tested at different time points (0, 1, 2, 3, 4, 5, and 6 h). The concentrations of IONPs used were (10, 30, and 60 µg/mL), and *Wormwood* extract (0.0035 g/mL) to evaluate the antibacterial activity, and Meropenem (10 µg/mL) as a control. We observed in the first hours a gradual decrease in absorption (λ_{max} 600 nm) with increasing the amount of treatment with IONPs, which confirms to us that IONPs caused harm to the bacteria, where we observed the death of the bacteria in the first hours (Fig. 17). Afterward, the absorption path changed, and there was little subsequent growth of the survivors after the initial killing phase. In contrast, this strong growth and recovery of bacteria is due to the low concentrations used, as bacterial death is directly related to the increase in the dose of the treatment (IONPs).

Our results showed that bacterial killing is highly dependent on concentration and time, as well as on the contribution of the active compounds of the *Wormwood* extract present on the surface of IONPs. Bacterial death is mostly explained by the production of reactive oxygen species. They lead to damage to the nucleic acids and proteins in the bacterial cells. IONPs interact with membrane proteins, causing oxidative stress, which results in protein degradation, membrane leakage, and higher permeability. All this ultimately leads to the death of the microorganism. In addition to disrupting the cell membrane of bacteria, it distorts the integrity of the structure and cellular function. As mentioned in a previous study, due to the complex structure of Gram-negative bacteria, IONPs are more effective against Gram-positive bacteria [120]. In contrast, the *Wormwood* extract alone showed significantly lower antibacterial activity than IONPs. This study is consistent with ours, despite the difference in metal; silver nanoparticles prepared with *Wormwood* showed up to 12 times greater antibacterial activity compared to the extract alone [134].

In addition, Meropenem at 10 µg/mL, applied as a minimum dose control, showed similar results with IONPs at 60 µg/mL, especially during the third and fourth hours of incubation, and the effect of meropenem was quite pronounced against *A. baumannii* throughout the incubation hours.

3.4.3. *The minimum inhibitory concentration (MIC) evaluation results*

Research into Iron oxide nanoparticles has flourished in biological sciences and materials science in recent years as a result of their diverse chemical and physical properties. The minimum inhibitory concentration (MIC) of IONPs is defined as the lowest concentration of the nanoparticles that inhibits the growth of bacteria, where no visible bacterial growth or rise in absorbance was observed, compared to the growth control [135].

In this study, the MIC of green-synthesized IONPs against different bacterial strains was determined using the broth culture dilution method at a range of IONP concentrations (10, 30, and 60 µg/mL) where significant effects were observed on all strains compared with controls.

3.4.3.1. Minimum inhibitory concentration of IONPs against pathogenic Staphylococcus aureus bacteria. Iron oxide nanoparticles have shown a significant antibacterial effect against Gram-positive (*S. aureus*) bacteria. The results clearly illustrate a concentration-dependent effect of IONPs (see Fig. 18). Among the tested concentrations, 60 µg/mL displayed the strongest antibacterial activity, followed by 30 µg/mL, whereas 10 µg/mL showed only a slight inhibitory effect compared to the untreated control samples. This dose-dependent behaviour is consistent with previous reports on metal oxide nanoparticles, where increased nanoparticle concentration enhances bacterial exposure and interaction, resulting in more pronounced antimicrobial effects [136].

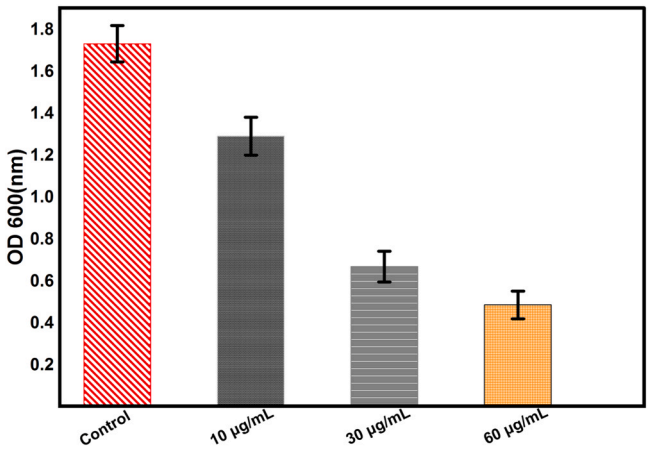

Fig. 18. The minimum bactericidal concentration of IONPs against *S. aureus* at different concentrations (10 µg/mL, 30 µg/mL, and 60 µg/mL). The control included only inoculated broth and was incubated for 24 h at 37 °C. The percentage of inhibition of *S. aureus* is treated by IONPs is shown.

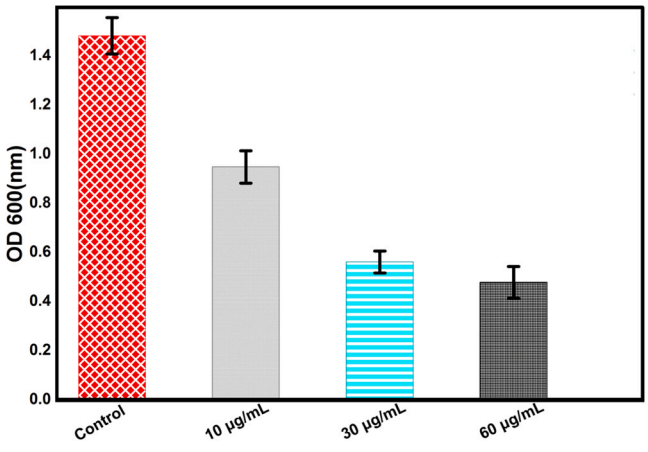

Fig. 19. The results of minimum bactericidal concentration IONPs against *A. baumannii* at different concentrations (10 µg/mL, 30 µg/mL, and 60 µg/mL). The control included only inoculated broth and was incubated for 24 h at 37 °C. The percentage of inhibition of *A. baumannii* treated with IONPs is shown.

The superior antibacterial activity observed at higher concentrations can be attributed to the increased availability of active NPs surface area, which improves contact with bacterial cells. IONPs are known to exert antibacterial effects via multiple mechanisms, including disruption of bacterial cell membranes, alteration of membrane permeability, generation of reactive oxygen species (ROS), metal ion release, and interference with intracellular metabolic processes [137]. At lower concentrations (10 µg/mL), these interactions may be insufficient to cause significant structural or metabolic damage, resulting in limited growth inhibition.

From Fig. 18, it can be seen that the optical absorption value at 600 nm for the control samples was 1.73 nm. A slight decrease in bacterial growth was observed at a concentration of (10 µg/mL) of IONPs, with the absorbance dropping to (1.29 nm), which is lower than the control group. While higher concentrations of IONPs (30 µg/mL) inhibited bacterial growth, the inhibition reached approximately half the absorbance of the control group (0.67 nm). The absorbance, which indicates the ability of nanoparticles to inhibit bacterial growth, is directly proportional to the concentration, consistent with the findings in [136].

In addition, the highest concentration (60 µg/mL) yielded a remarkably lower absorbance (0.48 nm) than all other concentrations tested, compared to the control group.

In summary, the antibacterial activity of IONPs against *S. aureus* showed a clear dose-dependent inhibition pattern. At a concentration of 10 µg/mL, around 26% growth inhibition was noted. Increasing the concentration to 30 µg/mL notably enhanced inhibition to approximately 62%, exceeding the 50% threshold (MIC_{50}). The inhibition reached approximately 72% at 60 µg/mL. However, 90% growth inhibition (MIC_{90}) was not achieved within the tested concentration range (10–60 µg/mL), demonstrating that higher concentrations would be required to reach complete bacteriostatic activity in the future.

3.4.3.2. MIC of IONPs against pathogenic A.baumannii bacteria. The minimum inhibitory concentration (MIC) of IONPs for *A. baumannii* at different concentrations (10, 30, and 60 µg/mL) was determined in this study.

It is well mentioned that the Iron oxide nanoparticles were active against gram-negative bacteria more than gram-positive bacteria according to Al-Rawi's investigation [135].

Herein, the results revealed a similarity in inhibition between *Staphylococcus aureus* and *A. baumannii*. The results showed that the optical density (OD) at 600 nm is concentration-dependent; the absorbance decreases as the nanoparticle concentration increases (see Fig. 19). Our results showed that the lowest concentration (10 µg/mL) produced an absorbance at (0.94 nm) compared to the control group, while the absorbance decreased to (0.56 nm) when the concentration increased to (30 µg/mL). At the highest concentration (60 µg/mL), the absorbance was significantly lower than both the control group and the other concentrations, reaching 0.49 nm. Therefore, these results confirm that the MIC of IONPs is (30 µg/mL) against *A. baumannii*. A study very similar to ours reported that the minimum MIC for Iron oxide nanoparticles for *P. mirabilis* and *A. baumannii* was 50 µg/mL [138].

IONPs against *A. baumannii* showed inhibition rates of approximately 37%, 63%, and 68% at the same concentrations mentioned above. In both strains, 30 µg/mL exceeded the 50% inhibition threshold and was thus regarded as the MIC_{50}. However, 90% inhibition was not reached within the evaluated concentration range (10–60 µg/mL), indicating that MIC_{90} is greater than 60 µg/mL. The comparison between inhibition percentages of IONPs against both strains is shown in Table 3.

The ability of IONPs to inhibit bacterial growth is attributed to the photocatalytic generation of reactive oxygen species, localized temperature increase, and vibrational damage caused by the magnetic field. These factors lead to bacterial detachment from the biofilm, damage to the bacterial cell wall, biofilm rupture, and fusion of different cells, resulting in either complete bacterial death or growth inhibition [138].

It is well mentioned that the Iron oxide nanoparticles were active against gram-negative more than gram-positive bacteria [135].

Interestingly, although both bacterial strains were susceptible to the green-synthesized IONPs, A. baumannii exhibited a greater sensitivity in comparison to *S. aureus*. This difference may be explained by the structural variations between Gram-negative and Gram-positive bacteria. A. baumannii, a Gram-negative bacterium, possesses a relatively thin peptidoglycan layer and an outer membrane rich in lipopolysaccharides, which can facilitate nanoparticle adhesion and penetration. In contrast, S. aureus, a Gram-positive bacterium, has a thick peptidoglycan cell wall, which may act as a physical barrier, reducing nanoparticle penetration and conferring relatively higher resistance.

It is revealed that Fe_2O_3 nanoparticles bind to the cell wall and even penetrate the cytoplasm, where they accumulate, producing vacuole formation and cell wall disruption. Furthermore, IONPs bind to the formate hydrogenlyase complex found in Gram negative bacteria cell walls, creating a gradient in the inner membrane that has a strong antimicrobial effect on these bacteria. As well as the shape and size of IONPs are suggested as key factors in explaining their bactericidal activity. Additionally, the enhanced antibacterial performance of IONPs is partly attributed to phytochemical coating agents extracted from the plant extract used in the green synthesis procedure. These bioactive

Table 3
Inhibition percentages of IONPs against *S. aureus* and *A. baumannii* after 24 h incubation.

Bacterial strain	Concentration (μg/mL)	OD600 (mean ± SD)	Inhibition (%)
S. aureus	Control	1.72 ± 0.01—	0%
	10	1.28 ± 0.04—	25.6%
	30	0.66 ± 0.03—	61.6%
	60	0.48 ± 0.05—	72.1%
A. baumannii	Control	1.48 ± 0.01	0%
	10	0.94 ± 0.06	36.5%
	30	0.55 ± 0.03	62.8%
	60	0.47 ± 0.04	68.2%

compounds synergistically inhibit bacterial growth by improving the dispersion and stability of the nanoparticles and destabilizing cell membranes, thereby improving bioavailability and antibacterial efficacy [4].

Overall, the results indicate that the environmentally friendly, manufactured iron oxide nanoparticles exhibit broad-spectrum antibacterial activity against both Gram-negative and Gram-positive bacteria, with a particularly strong effect against Acinetobacter baumannii. The concentration-dependent inhibition highlights the importance of dose optimization for effective antibacterial applications. These findings support the potential of green-synthesized iron oxide nanoparticles as promising antibacterial agents, especially against multidrug-resistant bacterial strains.

4. Conclusion

The study concluded that the biological synthesis of ionic nanoparticles (IONPs) proved to be a safer, more efficient, more sustainable, and more economical method. The aqueous extract of *Wormwood* effectively accelerated the formation of nanoparticles through its powerful capping and stabilizing agents. The biosynthesized IONPs were characterized by UV-Vis spectroscopy, FTIR, XRD, zeta, DLS, and TEM analysis. Transmission electron microscopy (TEM) revealed that the IONPs were spherical with a size of 17 ± 7.4 nm, and the DLS results also confirmed a small size (33 ± 2.5), which totally agrees with TEM results. The zeta value of IONPs was recorded at 44.32 mV, indicating high stability. While X-ray diffraction (XRD) analysis confirmed the highly crystalline nature of α-Fe_3O_4.

The antioxidant activity of IONPs using DPPH increased gradually with increasing IONP concentration. In addition, the biological activity of IONPs functionalized with *Wormwood* leaf extract was monitored against *Acinetobacter baumannii* and *Staphylococcus aureus* bacteria using time-kill curves. The antibacterial activity was found to be dependent on the concentration of IONPs and different bacterial species. The environmentally friendly, manufactured IONPs exhibit broad-spectrum antibacterial activity against both Gram-negative and Gram-positive bacteria, and the values of MIC were 30 μg/mL against both types of bacteria tested. These findings may encourage researchers to apply this type of safe nanoparticle in the medical field in the future instead of traditional drugs, particularly against resistant bacteria.

Ethics

This study did not require ethical approval from a human subject or animal welfare committee.

Funding

This research received no external funding.

CRediT authorship contribution statement

Wanisa Abdussalam-Mohammed: Supervision, Conceptualization, Visualization, Writing – original draft, Data curation, Formal analysis, Writing – review & editing. **Adel Younes:** Resources, Writing – original draft, Methodology, investigation, Formal analysis, Data curation, Software, Visualization, Writing – review & editing. **Mashael M. Alshaikh:** Investigation, Writing – review & editing, Software, Resources, Visualization. **Moussa Khlifa:** Investigation, Software, Resources. **Walaa Al-Masri:** Investigation, Software, Resources, Visualization, Writing – review & editing. **Pawan Shah:** Resources, Visualization, Software. **Ajaya Bhattarai:** Funding acquisition, Visualization, Writing – review & editing.

Declaration of Competing Interest

The authors declare that they have no known competing financial interests or personal relationships that could have appeared to influence the work reported in this paper.

Acknowledgments

The authors would like to thank the Department of Chemistry, Sebha University, Sebha /Libya and the University of Tripoli for their support

Data accessibility

Data supporting the findings of this study are available in the electronic supplementary materials.

Appendix A. Supporting information

Supplementary data associated with this article can be found in the

online version at doi:10.1016/j.nxmate.2026.101972.

References

[1] E. Amstad, M. Textor, E. Reimhult, Stabilization and functionalization of iron oxide nanoparticles for biomedical applications, J. Nanoscale 3 (7) (2011) 2819–2843.

[2] S. Sultana, N. Alzahrani, R. Alzahrani, W. Alshamrani, W. Aloufi, A. Ali, S. Najib, N.A. Siddiqui, Stability issues and approaches to stabilised nanoparticles based drug delivery system, J. Drug Target. 28 (5) (2020) 468–486.

[3] P. Karpagavinayagam, C. Vedhi, Green synthesis of iron oxide nanoparticles using Avicennia marina flower extract, J. Vac. 160 (2019) 286–292.

[4] J. Zúñiga-Miranda, J. Guerra, A. Mueller, A. Mayorga-Ramos, S.E. Carrera-Pacheco, C. Barba-Ostria, J. Heredia-Moya, L.P. Guamán, Iron oxide nanoparticles: green synthesis and their antimicrobial activity, J. Nanomater. 13 (22) (2023) 2919.

[5] H.A. Mohammed, L.S. Eddine, G.G. Hasan, S. Meneceur, C. Salmi, J.A. A. Abdullah, M.M. Abdullah, F. Menaa, Efficient removal of Heavy metals, dyes, and contaminants from Industrial Wastewater using Chitosan-Coated Fe3O4 nanocomposites: biosynthesis, Characterizations, and performance evaluation, Biomass-.-. Convers. Biorefinery 14 (23) (2024) 30719–30734.

[6] S. Salim, N. Hari, S. Sudhi, A.J. Nair, Green synthesis, characterisation and bioactivity of iron oxide nanoparticles using myristica fragrans leaf extract, J. Microbe (2025) 100481.

[7] K.M. Kumar, B.K. Mandal, K.S. Kumar, P.S. Reddy, B. Sreedhar, Biobased green method to synthesise palladium and iron nanoparticles using Terminalia chebula aqueous extract, J. Spectrochim. Acta Part A Mol. Biomol. Spectrosc. 102 (2013) 128–133.

[8] A. Bouafia, S.E. Laouini, Green synthesis of iron oxide nanoparticles by aqueous leaves extract of Mentha pulegium L.: effect of ferric chloride concentration on the type of product, J. Mater. Lett. 265 (2020) 127364.

[9] M. Senthil, C. Ramesh, Biogenic synthesis of Fe3O34 nanoparticles using Tridax procumbens leaf extract and its antibacterial activity on Pseudomonas aeruginosa, 01/01, Dig. J. Nanomater. Biostructures 7 (2012) 1655–1661, 01/01.

[10] E.-A. Moacă, C.G. Watz, C. Păcurariu, L.B. Tudoran, R. Ianoș, V. Socoliuc, et al., Biosynthesis of iron oxide nanoparticles: physico-chemical characterization and their In vitro cytotoxicity on healthy and tumorigenic cell lines, J. Nanomater. 12 (12) (2022) 2012.

[11] M. N. Abuhadra, M. H. Mahklouf, R. S. Essokne, A new record Artemisia vulgaris L. (Asteraceae) for the flora of Libya, Am. J. Life Sci. Res. 5 (3) (2017) 83–88.

[12] M. Hu, G. Feng, L. Xie, X. Shi, B. Lu, Y. Li, S. Shi, J. Zhang, Green and efficient extraction of wormwood essential oil using natural deep eutectic solvent: process optimization and compositional analysis, J. Mol. Liq. 382 (2023) 121977.

[13] S.M. Aldossari, L.U. Rehman, I. Ahmad, M. Aslam, F. Fozia, M. Mohany, M. Milosevic, S.S. Al-Rejaie, M.A. Aboul-Soud, Phytosynthesized iron oxide nanoparticles using aqueous extract of Saccharum arundinaceum (hardy sugar cane), their characterizations, antiglycation, and cytotoxic activities, J. Am. Chem. Soc. Omega 8 (44) (2023) 41214–41222.

[14] M.J. Towler, P.J. Weathers, Variations in key artemisinic and other metabolites throughout plant development in Artemisia annua L. for potential therapeutic use, J. Ind. Crops Prod. 67 (2015) 185–191.

[15] B. Ivanescu, L. Vlase, C. Lungu, A. Corciova, HPLC analysis of phenolic compounds from Artemisia species, Eur. Chem. Bull. 5 (4) (2016) 119–123.

[16] B. Ndaba, A. Roopnarain, B. Vatsha, S. Marx, M. Maaza, Synthesis, characterization, and evaluation of Artemisia afra-mediated iron nanoparticles as a potential nano-priming agent for seed germination, J. Am. Chem. Soc. Agric. Sci. & Technol. 2 (6) (2022) 1218–1229.

[17] M.El Ghanjaoui, A. Soufi, Y. Kadmi, N. Barka, H. Tounsadi, Sustainable synthesized iron oxide nanoparticles as a highly efficient material for degradation of dyes: characterization and statistical optimization approach, J. Chemosphere 376 (2025) 144266.

[18] M.A.J. Kouhbanani, N. Beheshtkhoo, A.M. Amani, S. Taghizadeh, V. Beigi, A. Z. Bazmandeh, N. Khalaf, Green synthesis of iron oxide nanoparticles using Artemisia vulgaris leaf extract and their application as a heterogeneous Fenton-like catalyst for the degradation of methyl orange, J. Mater. Res. Express 5 (11) (2018) 115013.

[19] B. Shelembe, R. Moodley, H. Chenia, vitro antibacterial and cytotoxic activity of zinc oxide, iron oxide and silver nanoparticles synthesised from Artemisia afra, South Afr. J. Chem. 77 (2023) 119–125.

[20] N.M. Hamdy, A.A. Boseila, A. Ramadan, E.B. Basalious, Iron oxide nanoparticles-plant insignia synthesis with favorable biomedical activities and less toxicity, in the "era of the-green": a systematic review, J. Pharm. 14 (4) (2022) 844.

[21] J. Sandhya, S. Kalaiselvam, Biogenic synthesis of magnetic iron oxide nanoparticles using inedible Borassus flabellifer seed coat: characterization, antimicrobial, antioxidant activity and in vitro cytotoxicity analysis, J. Mater. Res. Express 7 (1) (2020) 015045.

[22] F. Alzoubi, O.A. Noqta, T. AlZoubi, H. AlJabaly, H. Alkhateeb, M. Alqadi, G. Makhadmeh, Exploring the impact of pH on the properties of citric acid-coated iron oxide nanoparticles as high-performance T2 contrast agent for MRI applications, J. Results Eng. 18 (2023) 101206.

[23] W.I.W. Ismail, Biogenic silver nanoparticles (AgNPs) from Marphysa moribidii extract: optimization of synthesis parameters, Int. J. Technol. (2021).

[24] S. Ahmadi, C. Izanloo, Biosynthesis of iron oxide nanoparticles at different temperatures and its application for the removal of Zinc by plant mediated nanoparticle, as an eco-friendly nanoadsorbent, J. Results Chem. 6 (2023) 101192.

[25] E.M. Halawani, S.S. Alzahrani, S.M. Gad El-Rab, Biosynthesis strategy of gold nanoparticles and biofabrication of a novel amoxicillin gold nanodrug to overcome the resistance of multidrug-resistant bacterial pathogens MRSA and E. coli, J. Biomim. 8 (6) (2023) 452.

[26] R. Singh, TEM sample preparation for powder and liquid formulations. Transmission Electron Microscopy Sample Preparation: From Specimen to Micrograph, Springer, 2025, pp. 61–95.

[27] S. Mourdikoudis, R.M. Pallares, N.T. Thanh, Characterization techniques for nanoparticles: comparison and complementarity upon studying nanoparticle properties, J. Nanoscale 10 (27) (2018) 12871–12934.

[28] A.H. Gharbi, S.E. Laouini, H. Hemmami, A. Bouafia, M.T. Gherbi, I. Ben Amor, et al., Eco-friendly synthesis of Al2O3 nanoparticles: comprehensive characterization properties, mechanics, and photocatalytic dye adsorption study, Coatings 14 (7) (2024) 848.

[29] A.P. Malino, B.J. Kepel, F.D.H. Budiarso, F. Fatimawali, A.E. Manampiring, W. Bodhi, vitro test of antioxidant activity of leilem leaf ethanol extract (Clerodendrum minahassae) using DPPH and FRAP methods, Heca J. Appl. Sci. 2 (1) (2024) 27–34.

[30] L. de León Guerra, N. Padilla Montaño, L. Moujir, Interference of celastrol with cell wall synthesis and biofilm formation in staphylococcus epidermidis, J. Antibiot. 14 (1) (2025) 26.

[31] E. Hoseinzadeh, P. Makhdoumi, P. Taha, H. Hossini, M. Pirsaheb, S. Omid Rastegar, J. Stelling, A review of available techniques for determination of nano-antimicrobials activity, Toxin Rev. 36 (1) (2017) 18–32.

[32] A. Bouafia, S.E. Laouini, A. Khelef, M.L. Tedjani, F. Guemari, Effect of ferric chloride concentration on the type of magnetite (Fe3O4) nanoparticles biosynthesized by aqueous leaves extract of Artemisia and assessment of their antioxidant activities, J. Clust. Sci. 32 (4) (2021) 1033–1041.

[33] D. Aksu Demirezen, Ş. Yılmaz, D. Demirezen Yılmaz, Y.Ş. Yıldız, Green synthesis of iron oxide nanoparticles using Ceratonia siliqua L. aqueous extract: improvement of colloidal stability by optimizing synthesis parameters, and evaluation of antibacterial activity against Gram-positive and Gram-negative bacteria, Int. J. Mater. Res. 113 (10) (2022) 849–861.

[34] A. Mishra, M. Sardar, Isolation of genomic DNA by silane-modified iron oxide nanoparticles, J. Nanotechnol. Nov. Perspect. Prospects (2015) 309–315.

[35] A. Sani, D. Hassan, G.Q. Chanihoon, D.V. Melo Máximo, E.P. Sanchez-Rodriguez, Green chemically synthesized iron oxide nanoparticles–chitosan coatings for enhancing strawberry shelf-life, J. Polym. 16 (23) (2024) 3239.

[36] S. Khashan, S. Dagher, N. Tit, A. Alazzam, I. Obaidat, Novel method for synthesis of Fe3O4@ TiO2 core/shell nanoparticles, J. Surf. Coat. Technol. 322 (2017) 92–98.

[37] M. Yusefi, K. Shameli, O. Su Yee, S.-Y. Teow, Z. Hedayatnasab, H. Jahangirian, T. J. Webster, K. Kuča, Green synthesis of Fe3O4 nanoparticles stabilized by a Garcinia mangostana fruit peel extract for hyperthermia and anticancer activities, Int. J. Nanomed. (2021) 2515–2532.

[38] A. Ebrahiminezhad, A. Zare-Hoseinabadi, A. Berenjian, Y. Ghasemi, Green synthesis and characterization of zero-valent iron nanoparticles using stinging nettle (Urtica dioica) leaf extract, J. Green. Process. Synth. 6 (5) (2017) 469–475.

[39] S. Lohrasbi, M.A.J. Kouhbanani, N. Beheshtkhoo, Y. Ghasemi, A.M. Amani, S. Taghizadeh, Green synthesis of iron nanoparticles using Plantago major leaf extract and their application as a catalyst for the decolorization of azo dye, J. BioNanoScience 9 (2) (2019) 317–322.

[40] K. Shaik, S. Cole, Comparative study of crystallite size from XRD and TEM results for pure and V2O5 doped CdO-FePO4 composite nanopowders, Phys. Chem. Res. 11 (2) (2023) 241–251.

[41] N. Usov, O. Serebryakova, V. Tarasov, Interaction effects in assembly of magnetic nanoparticles, Nanoscale Res. Lett. 12 (1) (2017) 489.

[42] S. Saranya, K. Vijayarani, S. Pavithra, Green synthesis of iron nanoparticles using aqueous extract of musa ornata flower sheath against pathogenic bacteria, Indian J. Pharm. Sci. 79 (5) (2017).

[43] R.M. Abdallah, R.M. Al-Haddad, Optical and morphology properties of the magnetite (Fe3O4) nanoparticles prepared by green method, in: Journal of Physics: Conference Series, 1829, IOP Publishing, 2021 012022.

[44] E.-A. Moacă, I.Z. Pavel, C. Danciu, Z. Crăiniceanu, D. Minda, F. Ardelean, et al., Romanian wormwood (Artemisia absinthium L.): physicochemical and nutraceutical screening, J. Mol. 24 (17) (2019) 3087.

[45] G. Baranović, S. Šegota, Infrared spectroscopy of flavones and flavonols. Reexamination of the hydroxyl and carbonyl vibrations in relation to the interactions of flavonoids with membrane lipids, J. Spectrochim. Acta Part A Mol. Biomol. Spectrosc. 192 (2018) 473–486.

[46] A.S. Mamatova, I. Korona-Glowniak, K. Skalicka-Woźniak, A. Józefczyk, K. K. Wojtanowski, T. Baj, Z.B. Sakipova, A. Malm, Phytochemical composition of wormwood (Artemisia gmelinii) extracts in respect of their antimicrobial activity, BMC Complement. Altern. Med. 19 (1) (2019) 288.

[47] B. Kumar, K. Smita, S. Galeas, V.H. Guerrero, A. Debut, L. Cumbal, One-pot biosynthesis of maghemite (γ-Fe2O3) nanoparticles in aqueous extract of Ficus carica fruit and their application for antioxidant and 4-nitrophenol reduction, J. Waste Biomass-.-. Valoriz. 12 (7) (2021) 3575–3587.

[48] S. Chihi, A. Bouafia, S. Meneceur, S.E. Laouini, R.Z. Ahmed, Effect of precursor concentration on the bandgap energy and particles size for green synthesis of hematite α-Fe2O3 nanoparticles by the aqueous extract of Moltkia ciliata and evaluation of the antibacterial activity, Biomass-.-. Convers. Biorefinery 14 (23) (2024) 30369–30382.

[49] T. Girardet, S. Diliberto, C. Carteret, F. Cleymand, S. Fleutot, Determination of the percentage of magnetite in iron oxide nanoparticles: a comparison between mössbauer spectroscopy and Raman spectroscopy, Solid State Sci. 143 (2023) 107258.
[50] S. Kamsonlian, V. Agarwal, A. Gaur, J.-W. Park, Fe-nanoparticle amalgamation using lagenaria siceraria leaf aqueous extract with focus on dye removal and antibacterial efficacy, J. Korean Chem. Eng. Res. 61 (2) (2023) 287–295.
[51] A. Kachhawaha, M. Elizabeth, P. Hari, A. Rajan, N. Verma, Green synthesis and antibacterial evaluation of iron oxide nanoparticles using Clitoria ternatea flowers, Biomed. Pharmacol. J. 18 (1) (2025) 749–759.
[52] A. Gallo-Cordova, M. d P. Morales, E. Mazarío, Effect of the surface charge on the adsorption capacity of chromium (VI) of iron oxide magnetic nanoparticles prepared by microwave-assisted synthesis, J. Water 11 (11) (2019) 2372.
[53] I.T. Lucas, S. Durand-Vidal, E. Dubois, J. Chevalet, P. Turq, Surface charge density of maghemite nanoparticles: Role of electrostatics in the proton exchange, J. Phys. Chem. C. 111 (50) (2007) 18568–18576.
[54] V.V. Makarov, S.S. Makarova, A.J. Love, O.V. Sinitsyna, A.O. Dudnik, I. V. Yaminsky, M.E. Taliansky, N.O. Kalinina, Biosynthesis of stable iron oxide nanoparticles in aqueous extracts of Hordeum vulgare and Rumex acetosa plants, J. Langmuir 30 (20) (2014) 5982–5988.
[55] H. Muthukumar, M. Matheswaran, Amaranthus spinosus leaf extract mediated FeO nanoparticles: physicochemical traits, photocatalytic and antioxidant activity, J. Am. Chem. Soc. Sustain. Chem. & Eng. 3 (12) (2015) 3149–3156.
[56] A. Kmita, D. Lachowicz, J. Żukrowski, M. Gajewska, W. Szczerba, J. Kuciakowski, S. Zapotoczny, M. Sikora, One-step synthesis of long term stable superparamagnetic colloid of zinc ferrite nanorods in water, J. Mater. 12 (7) (2019) 1048.
[57] A. Adhikari, K. Chhetri, D. Acharya, B. Pant, A. Adhikari, Green synthesis of iron oxide nanoparticles using Psidium guajava L. leaves extract for degradation of organic dyes and anti-microbial applications, Catalysts 12 (10) (2022) 1188.
[58] S. Shukla, A. Jadaun, V. Arora, R.K. Sinha, N. Biyani, V. Jain, vitro toxicity assessment of chitosan oligosaccharide coated iron oxide nanoparticles, Toxicol. Rep. 2 (2015) 27–39.
[59] T. Yildiz, R. Gu, S. Zauscher, T. Betancourt, Doxorubicin-loaded protease-activated near-infrared fluorescent polymeric nanoparticles for imaging and therapy of cancer, Int. J. Nanomed. (2018) 6961–6986.
[60] Y.S. Kim, H.J. Lee, P. Govindaiah, W. Son, W.-G. Koh, I.W. Cheong, J.H. Kim, Preparation of Fe3O4-embedded poly (styrene)/poly (thiophene) core/shell nanoparticles and their hydrogel patterns for sensor applications, J. Mater. 7 (1) (2014) 195–205.
[61] V.K. Yadav, D. Ali, S.H. Khan, G. Gnanamoorthy, N. Choudhary, K.K. Yadav, V. N. Thai, S.A. Hussain, S. Manhrdas, Synthesis and characterization of amorphous iron oxide nanoparticles by the sonochemical method and their application for the remediation of heavy metals from wastewater, J. Nanomater. 10 (8) (2020) 1551.
[62] J. Dietrich, A. Enke, N. Wilharm, R. Konieczny, A. Lotnyk, A. Anders, S.G. Mayr, Energetic electron-assisted synthesis of tailored magnetite (Fe3O4) and maghemite (γ− Fe2O3) nanoparticles: structure and magnetic properties, J. Nanomater. 13 (5) (2023) 786.
[63] A.R. Chakraborty, F.T.Z. Toma, K. Alam, S.B. Yousuf, K.S. Hossain, Influence of annealing temperature on Fe_2O_3 nanoparticles: Synthesis optimization and structural, optical, morphological, and magnetic properties characterization for advanced technological applications, Heliyon 10 (21) (2024).
[64] R.M. Dragoman, M. Grogg, M.I. Bodnarchuk, P. Tiefenboeck, D. Hilvert, D. N. Dirin, M.V. Kovalenko, Surface-engineered cationic nanocrystals stable in biological buffers and high ionic strength solutions, J. Chem. Mater. 29 (21) (2017) 9416–9428.
[65] E.A. Meza Ramírez, A. Pérez Centeno, E. Campos-González, E. Camps, J. G. Quiñones Galván, Synthesis and characterization of Fe_2O_3 nanoparticles via pulsed laser ablation in liquids: effects of solvent and laser fluence, Sci. Rep. 15 (1) (2025) 36641.
[66] H. Etemadi, P.G. Plieger, Improvements in the organic-phase hydrothermal synthesis of monodisperse M x Fe3–x O4 (M= Fe, Mg, Zn) spinel nanoferrites for magnetic fluid hyperthermia application, ACS Omega 5 (29) (2020) 18091–18104.
[67] O. Milkovič, J. Gamcová, M. Sopko, I. Škorvánek, Structure and magnetic properties of iron/iron-oxide nanoparticles prepared by precipitation from solid state solution, Acta Phys. Pol. A 131 (4) (2017) 747–749.
[68] D. Egea-Benavente, C. Díaz-Ufano, Á. Gallo-Cordova, F.J. Palomares, J.L. Cuya Huaman, D.F. Barber, M. d P. Morales, J. Balachandran, Cubic mesocrystal magnetic iron oxide nanoparticle formation by oriented aggregation of cubes in organic media: a rational design to enhance the magnetic hyperthermia efficiency, J. Am. Chem. Soc. Appl. Mater. & Interfaces 15 (27) (2023) 32162–32176.
[69] H.I. Adamu, M.A. Richard, A.O. Olaniyi, Orange peel-mediated synthesis of Fe3O4 nanoparticles for the removal of ibuprofen from domestic wastewater, 12/30, BIMA JOURNAL SCIENCE TECHNOLOGY (2536-6041) 8 (4A) (2024) 138–164, 12/30.
[70] M. Ali, B. Kim, K. D. Belfield, D. Norman, M. Brennan, G.S. Ali, Green synthesis and characterization of silver nanoparticles using Artemisia absinthium aqueous extract—a comprehensive study, Journal Materials Science Engineering C 58 (2016) 359–365.
[71] N. Basavegowda, A. Idhayadhulla, Y.R. Lee, Preparation of Au and Ag nanoparticles using Artemisia annua and their in vitro antibacterial and tyrosinase inhibitory activities, Journal Materials Science Engineering C 43 (2014) 58–64.
[72] F.N. Alharbi, Z.M. Abaker, S.Z.A. Makawi, Phytochemical substances—mediated synthesis of zinc oxide nanoparticles (ZnO NPS), J. Inorg. 11 (8) (2023) 328.
[73] B. Karimi, M. Mardani, J. Kaboutari, M. Javdani, J. Albadi, S. Shirian, Green synthesis of copper oxide nanoparticles using Artemisia annua aqueous extract and its characterization, antioxidant, and burn wound healing activities, J. Chem. Pap. 78 (1) (2024) 231–243.
[74] O. Louafi, A. Khelef, S. Zeroual, S.E. Laouini, M.L. Tedjani, Effect of nickel nitrate concentration on the size of nickel oxide nanoparticles bio-synthesized by Artemisia herba-alba aqueous leaves extract and improving their antioxidant activities, J. Inorg. Organomet. Polym. Mater. 32 (3) (2022) 1116–1128.
[75] I.K.R. Kgosiemang, A.M. Adegoke, S.S. Mashele, M.P. Sekhoacha, Green synthesis of Iron oxide and Iron dioxide nanoparticles using Euphorbia tirucalli: characterization and antiproliferative evaluation against three breast cancer cell lines, J. Exp. Nanosci. 18 (1) (2023) 2276276.
[76] S.K. Filippov, R. Khusnutdinov, A. Murmiliuk, W. Inam, L.Y. Zakharova, H. Zhang, V.V. Khutoryanskiy, Dynamic light scattering and transmission electron microscopy in drug delivery: a roadmap for correct characterization of nanoparticles and interpretation of results, J. Mater. Horiz. 10 (12) (2023) 5354–5370.
[77] Z. Ahmad, A. Rauf, H. Zhang, M. Ibrahim, N. Muhammad, Y.S. Al-Awthan, O. S. Bahattab, Green synthesis and multifaceted characterization of iron oxide nanoparticles derived from Senna bicapsularis for enhanced in vitro and in vivo biological investigation, J. Green. Process. Synth. 13 (1) (2024) 20240001.
[78] K. Rajendran, V. Karunagaran, B. Mahanty, S. Sen, Biosynthesis of hematite nanoparticles and its cytotoxic effect on HepG2 cancer cells, Int. J. Biol. Macromol. 74 (2015) 376–381.
[79] N.A. Zakariya, S. Majeed, W.H.W. Jusof, Investigation of antioxidant and antibacterial activity of iron oxide nanoparticles (IONPS) synthesized from the aqueous extract of Penicillium spp, J. Sens. Int. 3 (2022) 100164.
[80] J. Iqbal, B. Abbasi, T. Mahmood, S. Hameed, A. Munir, S. Kanwal, Green synthesis and characterizations of Nickel oxide nanoparticles using leaf extract of Rhamnus virgata and their potential biological applications, 05/28, J. Appl. Organomet. Chem. (2019), 05/28.
[81] J. Choi, B.H. Kim, Ligands of nanoparticles and their influence on the morphologies of nanoparticle-based films, J. Nanomater. 14 (20) (2024) 1685.
[82] A. Heuer-Jungemann, N. Feliu, I. Bakaimi, M. Hamaly, A. Alkilany, I. Chakraborty, et al., The role of ligands in the chemical synthesis and applications of inorganic nanoparticles, J. Chem. Rev. 119 (8) (2019) 4819–4880.
[83] R. Kowalski, G. Kowalska, Phenolic acid contents in fruits of aubergine (solanum melongena L.), Pol. J. Food Nutr. Sci. 55 (1) (2005) 37–42.
[84] S.Y. Keskin, A. Avcı, H.F.F. Kurnia, Analyses of phytochemical compounds in the flowers and leaves of Spiraea japonica var. fortunei using UV–VIS, FTIR, and LC-MS techniques, Heliyon 10 (3) (2024).
[85] P.R.S. Baabu, H.K. Kumar, M.B. Gumpu, J. Babu K, A.J. Kulandaisamy, J.B. B. Rayappan, Iron oxide nanoparticles: a review on the province of its compounds, properties and biological applications, J. Mater. 16 (1) (2022) 59.
[86] Y. He, Y. Miao, C. Li, S. Wang, L. Cao, S. Xie, G. Yang, B. Zou, C. Burda, Size and structure effect on optical transitions of iron oxide nanocrystals, J. Phys. Rev. BCondens. Matter Mater. Phys. 71 (12) (2005) 125411.
[87] K.-C. Lee, S.-J. Lin, C.-H. Lin, C.-S. Tsai, Y.-J. Lu, Size effect of Ag nanoparticles on surface plasmon resonance, J. Surf. Coat. Technol. 202 (22-23) (2008) 5339–5342.
[88] P.K. Ngumbi, S.W. Mugo, J.M. Ngaruiya, Determination of gold nanoparticles sizes via surface plasmon resonance, Int. Organ. Sci. J. Appl. Chem. 11 (7) (2018) 25–29.
[89] M.S.H. Bhuiyan, M.Y. Miah, S.C. Paul, T.D. Aka, O. Saha, M.M. Rahaman, M.J. I. Sharif, O. Habiba, M. Ashaduzzaman, Green synthesis of iron oxide nanoparticle using Carica papaya leaf extract: application for photocatalytic degradation of remazol yellow RR dye and antibacterial activity, Heliyon 6 (8) (2020).
[90] R. Yadwade, S. Kirtiwar, B. Ankamwar, A review on green synthesis and applications of iron oxide nanoparticles, J. Nanosci. Nanotechnol. 21 (12) (2021) 5812–5834.
[91] A. Erdoğan, O. Kizilaslan, Comparison of long-term atmospheric aging between Fe 3 O 4 and PEG-protected Fe 3 O 4 nanoparticles, J. Am. Chem. Soc. Omega 10 (45) (2025) 54757–54763.
[92] M. Sathishkumar, K. Sneha, S. Won, C.-W. Cho, S. Kim, Y.-S. Yun, Cinnamon zeylanicum bark extract and powder mediated green synthesis of nano-crystalline silver particles and its bactericidal activity, J. Colloids Surf. B Biointerfaces 73 (2) (2009) 332–338.
[93] L. Deblock, E. Goossens, R. Pokratath, K. De Buysser, J. De Roo, Mapping out the aqueous surface chemistry of metal oxide nanocrystals: carboxylate, phosphonate, and catecholate ligands, J. Am. Chem. Soc. Au 2 (3) (2022) 711–722.
[94] M.O. Besenhard, A.P. LaGrow, A. Hodzic, M. Kriechbaum, L. Panariello, G. Bais, et al., Co-precipitation synthesis of stable iron oxide nanoparticles with NaOH: new insights and continuous production via flow chemistry, J. Chem. Eng. J. 399 (2020) 125740.
[95] A. Yan, X. Liu, G. Qiu, H. Wu, R. Yi, N. Zhang, J. Xu, Solvothermal synthesis and characterization of size-controlled Fe3O4 nanoparticles, J. Alloy. Compd. 458 (1-2) (2008) 487–491.
[96] M.D. Nguyen, H.-V. Tran, S. Xu, T.R. Lee, Fe3O4 nanoparticles: structures, synthesis, magnetic properties, surface functionalization, and emerging applications, Appl. Sci. 11 (23) (2021) 11301.
[97] J.A.A. Abdullah, Á. Díaz-García, J.Y. Law, A. Romero, V. Franco, A. Guerrero, Quantifying the structure and properties of nanomagnetic iron oxide particles for

enhanced functionality through chemical synthesis, J. Nanomater. 13 (15) (2023) 2242.
[98] A. Abedini, A.R. Daud, M.A.A. Hamid, N.K. Othman, pH-dependent magnetic phase transition of iron oxide nanoparticles synthesized by gamma-radiation reduction method, J. Radioanal. Nucl. Chem. 301 (2) (2014) 399–407.
[99] M. Salehirozveh, P. Dehghani, I. Mijakovic, Synthesis, functionalization, and biomedical applications of iron oxide nanoparticles (IONPs), J. Funct. Biomater. 15 (11) (2024) 340.
[100] J.A.A. Abdullah, Á. Díaz-García, J.Y. Law, A. Romero, V. Franco, A. Guerrero, Sustainable nanomagnetism: investigating the influence of green synthesis and pH on iron oxide nanoparticles for enhanced biomedical applications, J. Polym. 15 (18) (2023) 3850.
[101] Y. Park, R.D. Whitaker, R.J. Nap, J.L. Paulsen, V. Mathiyazhagan, L.H. Doerrer, et al., Stability of superparamagnetic iron oxide nanoparticles at different pH values: experimental and theoretical analysis, J. Langmuir 28 (15) (2012) 6246–6255.
[102] S. Woo, S. Kim, H. Kim, Y.W. Cheon, S. Yoon, J.-H. Oh, J. Park, Charge-modulated synthesis of highly stable iron oxide nanoparticles for in vitro and in vivo toxicity evaluation, J. Nanomater. 11 (11) (2021) 3068.
[103] A. Avasthi, C. Caro, M.L. Garcia-Martin, M.P. Leal, Deciphering the parameters to produce highly reproducible and scalable iron oxide nanoparticles, J. React. Chem. & Eng. 8 (7) (2023) 1638–1653.
[104] A.V. Shibaev, P.V. Shvets, D.E. Kessel, R.A. Kamyshinsky, A.S. Orekhov, S. S. Abramchuk, A.R. Khokhlov, O.E. Philippova, Magnetic-field-assisted synthesis of anisotropic iron oxide particles: effect of pH, Beilstein J. Nanotechnol. 11 (1) (2020) 1230–1241.
[105] S.K. Bhakar, B. Sharma, S. Satapathy, P. Deshmukh, V. Srihari, R. Singh, S. Majumder, Optimizing synthesis parameters to achieve phase-pure superparamagnetic Fe3O4 nanoparticles for magnetic hyperthermia, BioNanoScience 15 (3) (2025) 508.
[106] L.P. Mona, S.P. Songca, P.A. Ajibade, Effects of temperature and precursor concentration on the morphological and optical properties of iron oxide nanoparticles, J. Chem. Afr. 7 (8) (2024) 4581–4591.
[107] P. Cheah, J. Qu, Y. Li, D. Cao, X. Zhu, Y. Zhao, The key role of reaction temperature on a polyol synthesis of water-dispersible iron oxide nanoparticles, J. Magn. Magn. Mater. 540 (2021) 168481.
[108] G.F. Goya, Handling the particle size and distribution of Fe3O4 nanoparticles through ball milling, Solid State Commun. 130 (12) (2004) 783–787.
[109] O.E. Cigarroa-Mayorga, I. Torres-Sandoval, M. d R. Munguía-Fuentes, Y. M. Hernández-Rodríguez, Influence of temperature on the structural evolution of iron–manganese oxide nanoparticles in the hydrothermal method, Crystals 15 (9) (2025) 808.
[110] Q. Li, C.W. Kartikowati, S. Horie, T. Ogi, T. Iwaki, K. Okuyama, Correlation between particle size/domain structure and magnetic properties of highly crystalline Fe3O4 nanoparticles, Sci. Rep. 7 (1) (2017) 9894.
[111] F. Chen, N. Ilyas, X. Liu, Z. Li, S. Yan, H. Fu, Size effect of Fe3O4 nanoparticles on magnetism and dispersion stability of magnetic nanofluid, Front. Energy Res. 9 (2021) 780008.
[112] O.I. Aruoma, Free radicals, oxidative stress, and antioxidants in human health and disease, J. Am. oil Chem. ' Soc. 75 (2) (1998) 199–212.
[113] R.I. Salganik, The benefits and hazards of antioxidants: controlling apoptosis and other protective mechanisms in cancer patients and the human population, J. Am. Coll. Nutr. 20 (sup5) (2001) 464S–472S.
[114] Y. Lang, N. Gao, Z. Zang, X. Meng, Y. Lin, S. Yang, Y. Yang, Z. Jin, B. Li, Classification and antioxidant assays of polyphenols: a review, J. Future Foods 4 (3) (2024) 193–204.
[115] D. Siwan, D. Nandave, M. Nandave, Artemisia vulgaris Linn: an updated review on its multiple biological activities, Future J. Pharm. Sci. 8 (1) (2022) 47.
[116] M. Aydın, Y. Özcan, S.K. Coşkun, M. Alpay, N.C. Coşkun, Treatment of burn wounds with a chitosan-based hydrogel dressing containing Artemisia absinthium L.: a comprehensive in vivo study, Int. J. Tradit. Complement. Med. Res. 5 (1) (2024) 54–64.
[117] M.J. Mohammed, U. Anand, A.B. Altemimi, V. Tripathi, Y. Guo, A. Pratap-Singh, Phenolic composition, antioxidant capacity and antibacterial activity of white wormwood (Artemisia herba-alba), J. Plants 10 (1) (2021) 164.
[118] Z.I. Ismael, R.S. Toma, H.S. Faizy, Phytochemical analysis and antioxidant activity of wormwood (Artemisia absinthium L.) as a comparative study between in vitro and in vivo plants, Kufa J. Agric. Sci. 16 (3) (2024) 1–10.
[119] R. Prakash, R. Bharti, A. Thakur, M. Verma, R. Sharma, Environmentally benign green approach for the synthesis of IONPs using vicia faba fruit extract and their antioxidant activities, J. Sustain. Chem. Eng. (2025) 11–21.
[120] M. Nadeem, R. Khan, N. Shah, I.R. Bangash, B.H. Abbasi, C. Hano, et al., A review of microbial mediated iron nanoparticles (IONPs) and its biomedical applications, J. Nanomater. 12 (1) (2021) 130.
[121] S. Sultana, T. Bhuyan, R. Saha, Antibacterial and antioxidant activities of iron nanoparticles synthesized using banana inflorescence leaf extract, J. Mater. Environ. 412 (397) (2024) 15.
[122] G. Rabani, M. Dilshad, A. Sohail, A. Salman, S. Ibrahim, I. Zafar, H.M. Arshad, Extracellular synthesis of iron oxide nanoparticles using an extract of bacillus circulans: characterization and in vitro antioxidant activity, J. Chem. 2023 (1) (2023) 4659034.
[123] L.L. Panigrahi, S. Satpathy, P. Samal, S. Shekhar, S.K. Prusty, M. Arakha, Biosynthesized iron oxide-nanoparticle encapsulated hydrogel functionalized with platelet-rich plasma (PRP) accelerates wound healing in an animal model, Nanoscale Adv. 7 (22) (2025) 7209–7225.
[124] V.S. Abdullah, K.Y.M. Amin, H.I.M. Amin, Plant-assisted synthesis, phytochemical profiling, and bioactivity evaluation of copper nanoparticles derived from tordylium trachycarpum (apiaceae), Biomolecules 15 (12) (2025) 1693.
[125] S.T. Shah, W.A. Yehye, O. Saad, K. Simarani, Z.Z. Chowdhury, A. A. Alhadi, L. A. Al-Ani, Surface functionalization of iron oxide nanoparticles with gallic acid as potential antioxidant and antimicrobial agents, Nanomaterials 7 (10) (2017) 306.
[126] L. Kumar, M. Bisen, K. Harjai, S. Chhibber, S. Azizov, H. Lalhlenmawia, D. Kumar, Advances in nanotechnology for biofilm inhibition, J. Am. Chem. Soc. Omega 8 (24) (2023) 21391–21409.
[127] Q. Ye, W. Chen, H. Huang, Y. Tang, W. Wang, F. Meng, H. Wang, Y. Zheng, Iron and zinc ions, potent weapons against multidrug-resistant bacteria, J. Appl. Microbiol. Biotechnol. 104 (12) (2020) 5213–5227.
[128] O.M. Bankole, K.I. Ojubola, O.S. Adanlawo, A.O. Adesina, I.O. Lawal, A. S. Ogunlaja, O.J. Achadu, Amoxicillin encapsulation on alginate/magnetite composite and its antimicrobial properties against gram-negative and positive microbes, J. BioNanoScience 12 (4) (2022) 1136–1149.
[129] E.T. Jayathilaka, J. Han, M. De Zoysa, I. Whang, Antimicrobial peptide octoprohibitin-encapsulated chitosan nanoparticles enhanced antibacterial activity against acinetobacter baumannii, J. Pharm. 16 (10) (2024) 1245.
[130] F. Al-Otibi, N.A. Alshammry, R.I. Alharbi, M.N. Bin-Jumah, M.M. AlSubaie, Silver nanoparticles of Artemisia sieberi extracts: chemical composition and antimicrobial activities, J. Plants 12 (11) (2023) 2093.
[131] M.V. Morone, F. Dell'Annunziata, R. Giugliano, A. Chianese, A. De Filippis, L. Rinaldi, et al., Pulsed laser ablation of magnetic nanoparticles as a novel antibacterial strategy against gram positive bacteria, J. Appl. Surf. Sci. Adv. 7 (2022) 100213.
[132] X. Dai, X. Wang, X. Chen, L. Ye, M. Wu, Fabrication of ultrasound-mediated cerium oxide nanoparticles for the examinations of human osteomyelitis and antibacterial activity, J. Appl. Nanosci. 11 (10) (2021) 2549–2560.
[133] N. Bala, M. Sarkar, M. Maiti, P. Nandy, R. Basu, S. Das, Phenolic compound-mediated single-step fabrication of copper oxide nanoparticles for elucidating their influence on anti-bacterial and catalytic activity, N. J. Chem. 41 (11) (2017) 4458–4467.
[134] Y. Park, H.J. Noh, L. Han, H.-S. Kim, Y.-J. Kim, J.S. Choi, C.-K. Kim, Y.S. Kim, S. Cho, Artemisia capillaris extracts as a green factory for the synthesis of silver nanoparticles with antibacterial activities, J. Nanosci. Nanotechnol. 12 (9) (2012) 7087–7095.
[135] M. Al-Rawi, N. Al-Mudallal, A. Taha, Determination of ferrous oxide nanoparticles minimum inhibitory concentration against local virulent bacterial isolates, Arch. Razi Inst. 76 (4) (2021) 795.
[136] A. Parmanik, P.P. Kothari, A. Bose, S. Biswas, Evaluation of antibacterial and antibiofilm activities of green-synthesized iron oxide nanoparticles using Cyperus rotundus extract as a reducing and stabilizing agent, Journal Materials Science Materials Medicine 36 (1) (2025) 60.
[137] D.-A. Mercan, D.-I. Tudorache, A.-G. Niculescu, L. Mogoantă, G.D. Mogoşanu, A. C. Bîrcă, et al., Antimicrobial coatings based on hybrid iron oxide nanoparticles, Nanomaterials 15 (9) (2025) 637.
[138] F.M. Abdulsada, N.N. Hussein, G.M. Sulaiman, A. Al Ali, M. Alhujaily, Evaluation of the antibacterial properties of iron oxide, polyethylene glycol, and gentamicin conjugated nanoparticles against some multidrug-resistant bacteria, J. Funct. Biomater. 13 (3) (2022) 138.